Report
**R-19-26**
September 2020

# Numerical study of the influence from deposited gamma radiation energy on canister temperature in the Spent Fuel Repository

**Peter Renström**

SVENSK KÄRNBRÄNSLEHANTERING AB

SWEDISH NUCLEAR FUEL
AND WASTE MANAGEMENT CO

Box 3091, SE-169 03 Solna
Phone +46 8 459 84 00
skb.se

SVENSK KÄRNBRÄNSLEHANTERING

ISSN 1402-3091
**SKB R-19-26**
ID 1719471

September 2020

# Numerical study of the influence from deposited gamma radiation energy on canister temperature in the Spent Fuel Repository

Peter Renström, AEC AB

*Keywords:* Heat, Radiation, Gamma, Spent fuel, Simulation, Cesium, Europium.

# Summary

Over the years, several numerical studies and calculations have been made of the spatial and transient temperature distribution in the canister and its surroundings after disposal of the KBS-3 canister with spent nuclear fuel in the final repository. In these studies the decay heat generation has conventionally been assumed to be produced entirely inside a certain confined geometrical space representing the fuel assembly. However, decay simulations of encapsulated arrays of spent fuel ongoing at Uppsala University show that a significant amount of energy is emitted via gamma radiation from the fuel assembly to other regions inside as well as outside the canister. The emitted energy will be deposited at these irradiated regions which will be heated up and act as secondary heat power sources external from the fuel assemblies.

The present report describes a study, based on results from the above simulations, of how much the calculated temperature at the copper shell and its close surroundings could possibly differ between conventional thermal analysis models and models in which the spatial distribution of secondary heat power sources emanating from deposited gamma radiation is taken into account. For these comparative thermal analyses, a one-dimensional finite element model consisting of a horizontal, radial piece at the canister's midplane is used to calculate the transient temperature distribution for a single canister located in the final repository. The calculations focus on the temperature development in the copper shell and buffer.

For the three different fuel configurations studied, SVEA96S, BWR8x8 and PWR17x17, the following can be concluded:

- radiation from Cesium and Europium together covers at least 95 % of the emitted gamma energy for cooling times 30 years and longer.

Furthermore, with the assumption that radiation from Cs and Eu covers a representative amount of the total emitted energy from gamma radiation at all levels, the following can be concluded:

- at the studied part of the canister, the midplane slab of 1 cm thickness, the amount of gamma energy deposited outside the canister is less than 0.2 % of the amount deposited inside the canister,
- the heat power from emitted gamma energy deposited outside the canister is small compared to the heat generation inside the canister,
- calculations of the temperature on and exterior of the copper shell made with the conventional model simplifications, in this case with the residual heat uniformly and entirely generated inside a radius of 300 mm, gives virtually the same results as if the spatial distribution of deposited energy from gamma radiation were taken into account,
- a model with all the deposited energy from gamma radiation hypothetically located in the copper shell still gives virtually the same temperatures on and exterior of the copper shell as the conventional model,
- a model with all the deposited energy from gamma radiation hypothetically located in the buffer would give a few degrees lower temperature on and exterior of the copper shell compared to the conventional model,
- the spatial distribution of deposited energy from gamma radiation does not affect the temperature on and exterior of the copper shell unless a significant amount of energy is deposited outside the canister
- it is not necessary to take the spatial distribution of deposited energy from gamma radiation into account when calculating the temperature on and exterior of the copper shell.

# Sammanfattning

Under årens lopp har åtskilliga beräkningar och numeriska analyser utförts av den rumsliga och transienta temperaturfördelningen i och kring kapseln med utbränt kärnbränsle efter deponering i slutförvaret enligt KBS-3-metoden. I dessa studier har produktionen av restvärme konventionellt antagits ske helt och hållet inom en fördefinierad avgränsad volym som har fått representera bränslet. Emellertid visar simuleringar av sönderfallande inkapslat bränsle som utförs vid Uppsala Universitet att en signifikant del av energin emitteras via gammastrålning från bränslet till andra områden både inuti och utanför kapseln. Den emitterade energin kommer att deponeras i dessa bestrålade områden vilka kommer att hettas upp och fungera som sekundära värmeeffektkällor utanför själva bränsleknippena.

Föreliggande rapport redovisar en studie baserad på ovanstående simuleringar av hur mycket den beräknade temperaturen i kopparhöljet och dess nära omgivning kan skilja sig åt mellan konventionella termiska analysmodeller och modeller där hänsyn tagits till sekundära värmekällor härrörande från deponerad gammastrålningsenergi. I dessa jämförande termiska analyser har en en-dimensionell finita element-modell bestående av en horisontell, radiell kil vid kapselns mittplan använts för att beräkna den transienta temperaturfördelningen för en enstaka kapsel placerad i slutförvaret. Beräkningarna fokuserar på temperaturutvecklingen i kopparhöljet och bufferten.

För de tre olika bränslekonfigurationerna som studerats, SVEA96S, BWR8x8 och PWR17x17, kan följande slutsatser dras:

- strålning från Cesium och Europium utgör tillsammans minst 95 % av den emitterade gammaenergin för 30 års kyltid och längre.

Med antagandet att strålning från Cs och Eu täcker en representativ mängd av den totala emitterade energin från gammastrålning på alla nivåer, kan dessutom följande slutsatser dras:

- för den studerade delen, skivan med en tjocklek på 1 cm i kapsens mittplan, är mängden gamma-energi som deponeras utanför kapseln mindre än 0,2 % av den mängd som deponeras inuti kapseln,
- värmeeffekten från gammastrålningsenergi som deponeras utanför kapseln är liten jämfört med värmeproduktionen inuti kapseln,
- beräkningar av temperaturen på och utanför kopparhöljet utförda med en konventionell modell-förenkling där restvärmen i sin helhet produceras uniformt innanför radien 300 mm ger i praktiken samma resultat som beräkningar där hänsyn tas till den rumsliga fördelningen av deponerad gammastrålningsenergi,
- en beräkningsmodell med all gammastrålningsenergi hypotetiskt lokaliserad i kopparhöljet ger praktiskt taget samma temperatur på och utanför kopparhöljet som en konventionell modell,
- en beräkningsmodell med all gammastrålningsenergi hypotetiskt lokaliserad i bufferten skulle ge ett fåtal grader lägre temperatur på och utanför kopparhöljet jämfört med en konventionell modell,
- den rumsliga fördelningen av deponerad gammastrålningsenergi påverkar inte temperaturen på och utanför kopparhöljet såvida inte en signifikant mängd energi deponeras utanför kapseln,
- det är inte nödvändigt att ta hänsyn till den rumsliga fördelningen av deponerad gammastrålnings-energi vid beräkning av temperaturen på och utanför kopparhöljet.

# Contents

# 1 Introduction

Spent nuclear fuel is planned to be deposited in a final repository some 500 m down in the bedrock within the KBS-3 method (Figure 1-1). At the time of deposition, and several decades afterwards, the spent fuel will generate heat due to residual radioactive decay.

Over the years, several numerical studies and calculations have been made of the spatial and transient temperature distribution in the canister and its surroundings after deposition in the final repository, for instance, Hökmark et al. (2009, 2010) and Ikonen (2009, 2017) to mention a few. In these studies the residiual heat generation from nuclear decay has conventionally been assumed to be produced entirely inside a certain confined geometrical space, usually the fuel assemblies, or more generally inside some pre-defined cylinder. In some studies it has been approximated by a linear heater representing the canister internals. However, decay simulations of encapsulated arrays of spent fuel ongoing at Uppsala University show that a significant amount of energy is emitted via gamma radiation from the fuel assemblies to other regions inside as well as outside the canister. The emitted energy will be deposited at these irradiated regions which will be heated up and act as secondary heat power sources external from the fuel assemblies. A brief description of these gamma ray simulations is made in Chapter 2.

The present report describes a study, based on results from the above simulations, of how much the calculated temperature on the copper shell and its close surroundings could possibly differ between conventional thermal analysis models and models in which the spatial distribution of secondary heat power sources emanating from deposited gamma radiation is taken into account. To do this, an axisymmetric model of a single Posiva-BWR canister presented by Ikonen (2017, p 58) is chosen as a reference for the conventional thermal modelling approach. For comparative thermal analyses, a one-dimensional finite element model consisting of a horizontal, radial piece at canister midplane, based on the same material properties and with the same thermal resistance as in Ikonen (2017), is built as described in Chapter 3. The finite element model is then used to calculate the transient temperature distribution for a single canister in the final repository, with focus on the copper shell and buffer, for a number of different heat source conditions. The results are presented in Chapter 4 with conclusions and discussion in Chapter 5 and Chapter 6 respectively.

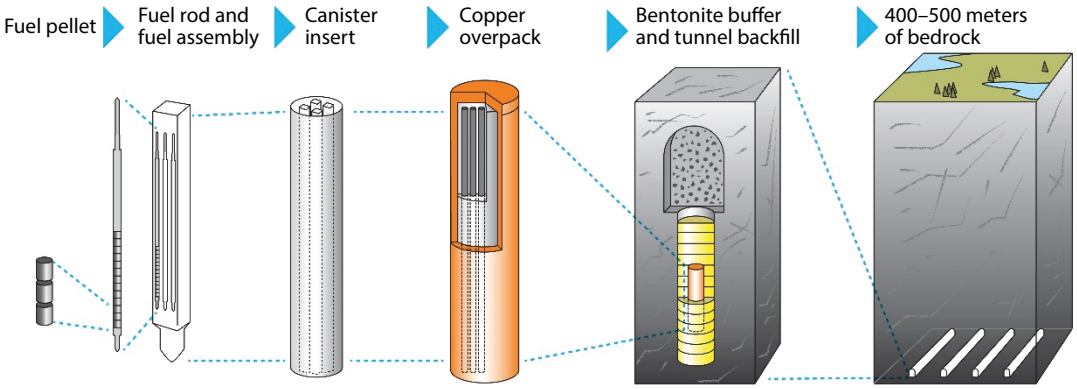


***Figure 1-1.*** *Schematic overview of the final repository according to the KBS-3 project (figure from Posiva Oy).*

# 2 Gamma ray simulations

## 2.1 General

Decaying spent nuclear fuel emits gamma radiation in the form of photons which deposit most of their energy in matter by particle interaction. The energy deposition for some selected encapsulated fuel types are being calculated by Uppsala University in extensive Monte-Carlo simulations of gamma ray trajectories.

## 2.2 Description of data from gamma ray simulations

The gamma ray simulation model used at Uppsala University represents a single canister standing vertical upright, located in the final repository. The computational space is divided into cubic voxels with 1 cm side. Result data for each voxel are filed in comma-separated values (CSV) format, where each data record consists of an *x-, y-, z*-coordinate together with a data value of energy (MeV). The data value for a certain voxel shall be interpreted as the calculated deposited gamma energy at that voxel per photon emitted from the fuel at the canister's horizontal midplane ($z$=0) in Figure 2-1.

Data files containing results from Uppsala University's gamma ray simulations of three different fuel configurations, SVEA96S, BWR8x8 and PWR17x17, for photons of energy 662 keV and 1 274 keV, the former representing Cs-137 (Cesium) and the latter Eu-154 (Europium), are listed in Table 2-1 and Appendix 1.

**Table 2-1. Result files from gamma ray simulations.**

| Filename | Fuel type | Burn-up |
|---|---|---|
| BWR1_1274keV.csv | SVEA96S | 40 MWd/kgU |
| BWR1_662keV.csv | SVEA96S | 40 MWd/kgU |
| BWR6_1274keV.csv | BWR8x8 | 40 MWd/kgU |
| BWR6_662keV.csv | BWR8x8 | 40 MWd/kgU |
| PWR8_1274keV.csv | PWR17x17 | 40 MWd/kgU |
| PWR8_662keV.csv | PWR17x17 | 40 MWd/kgU |

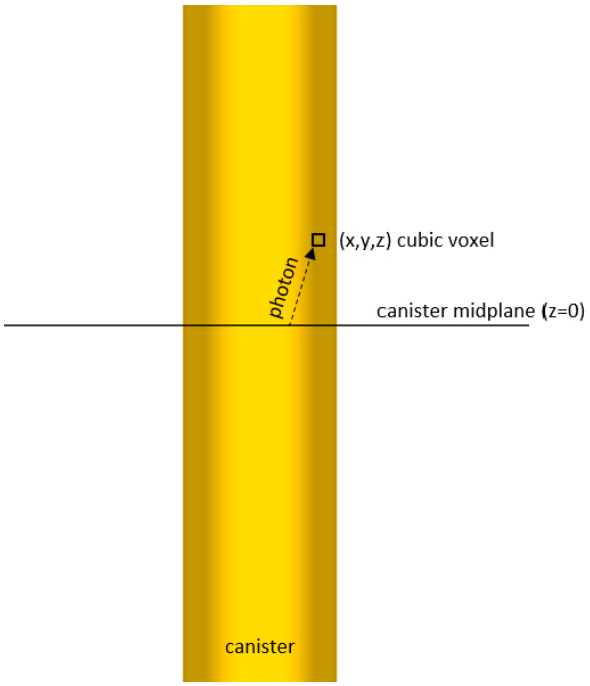


***Figure 2-1.*** *Illustration of gamma ray simulation model.*

The emitted gamma radiation intensity for the three fuel configurations is plotted in Figure 2-2. It can be seen that the number of photons at energy level 662 keV emitted from Cesium decay is dominant. Emission from Europium at 1 274 keV is also significant, and, moreover, at a higher energy level than Cesium, which means that photons can reach further out from the fuel before its energy is deposited. The radiation intensity is, however, almost 100 times lower than that from Cesium. By taking just these two energy levels into account, it is judged that a representative, although underestimated, amount of the emitted energy from gamma radiation at all levels is covered.

The coverage can be estimated by multiplying the gamma energy with the number of emitted photons to get the emitted energy for a each gamma energy level. For instance, according to Table A2-1, Cesium in SVEA96S 30 years after service emits: 0.662[MeV/photon] · 2.28E+14[photons/assembly/s] · 12[assemblies/canister] = 1.81E+15 MeV/canister/s = 290 W per canister. Analogously, Europium emits 4.9 W per canister, which in total means that radiation from Cesium and Europium together cover 95 % of the emitted gamma energy. Figure 2-3 suggests that an even larger part is covered by Cs and Eu, (43.60+1.13)W/44.90W = 99.6 %

In the final repository all energy emitted through gamma radiation will be deposited and thus will contribute to the total residual heat. Calculations made by Jansson (2002), Uppsala University, indicate that gamma radiation stands for about 24 % of the total residual heat power (Figure 2-3). With this relation adopted the heat power from deposited gamma energy and the total residual heat power for the three fuel configurations are shown in Table 2-2.

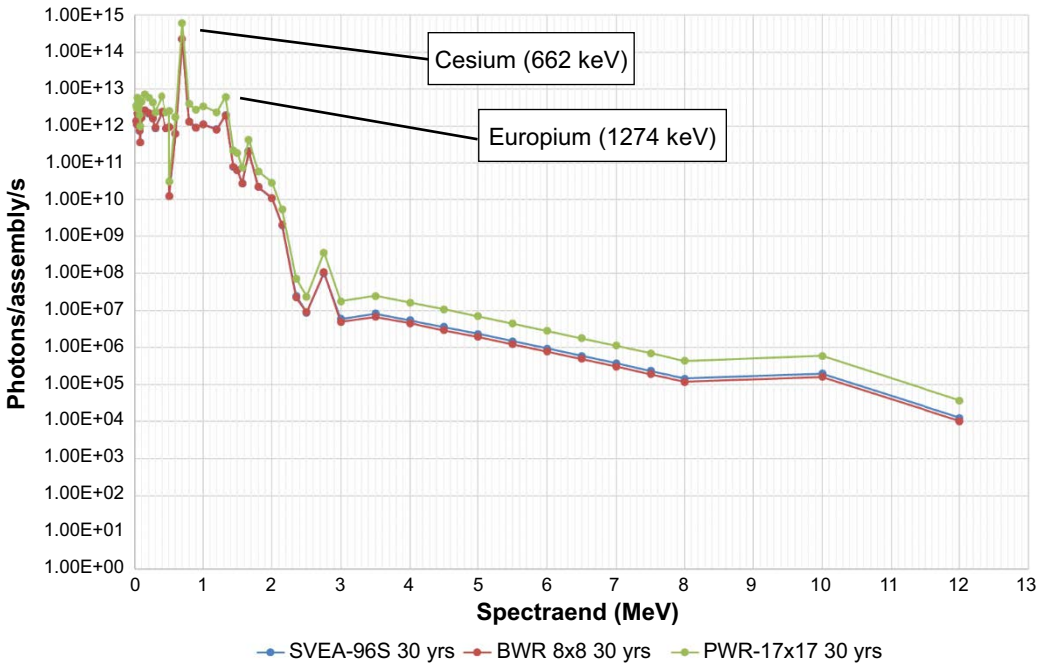


***Figure 2-2.*** *Emitted gamma radiation intensity for fuel 30 years after service as tabulated in Appendix 2 (note that the ratio between PWR and BWR intensities is about 3 since a PWR assembly contains roughly three times the fuel amount of a BWR assembly).*

| Isotope | Thermal power [W] | Gamma power [W] |
|---|---|---|
| kr85 | 0.43 | |
| sr90 | 9.54 | |
| y90 | 45.40 | |
| sb125 | | 0.002 |
| cs134 | 0.02 | 0.02 |
| cs137 | 14.46 | |
| ba137m | 48.20 | 43.60 |
| eu154 | 1.38 | 1.13 |
| pa233 | | 0.0001 |
| u237 | | 0.0001 |
| np239 | | 0.0091 |
| pu238 | 22.00 | 0.01 |
| pu239 | 1.94 | 0.0003 |
| pu240 | 4.00 | 0.001 |
| pu241 | 0.22 | 0.00 |
| am241 | 25.40 | 0.13 |
| am242 | | 0.0002 |
| am243 | 0.27 | 0.003 |
| cm242 | 0.05 | |
| cm243 | 0.11 | 0.002 |
| cm244 | 14.74 | 0.005 |
| **Total** | **188.15** | **44.90** |
| | | **23.9%** |

***Figure 2-3.*** *Total thermal and gamma power 30 years after service calculated with ORIGEN-S for a SKB-BWR assembly with 3 % initial 235U enrichment and 40 GWd/tU burnup over four fuel cycles (Jansson 2002). Power originating from Cs in blue, from Eu in orange.*

**Table 2-2. Gamma power compared to total residual heat power per canister for the simulated fuel 30 years after service assuming that gamma power from Cs and Eu is 24 % of total heat power.**

| | SVEA96-S | | BWR8x8 | | PWR17x17 | |
|---|---|---|---|---|---|---|
| | Cs | Eu | Cs | Eu | Cs | Eu |
| Emitted as gamma energy | 290 W | 4.9 W | 287 W | 4.7 W | 259.6 | 5.0 |
| Total | 1 229 W | | 1 215 W | | 1 103 W | |

## 2.3 Data processing for thermal analysis

Due to the nature of the gamma radiation model the deposited energy results are most accurate close to the canister's midplane. Therefore, the thermal analysis is chosen to focus in that region as well.

Assuming that all energy deposited at a certain voxel will turn into heat, the data files in Table 2-1 are processed to create appropriate input data for the thermal analysis described in Chapter 3[1]. This is done by summing the deposited energy data values over the fuel height, multiplied by the radiation intensity, to get the volumetric heat generation distribution at canister midplane shown in Figure 2-4 to Figure 2-11. Contours of the canister with buffer and rock are shown in the figures at the upper right quadrant as a geometrical reference.

[1] Since the data files from the gamma ray simulations are way too big to handle in, for instance, Excel 2016, an in-house programming tool has been developed for this.

In order to get the deposited energy for each voxel at the horizontal slab of thickness 1 cm at canister midplane, per photon emitted from any fuel in the canister, the energy data values for each coordinate pair ($x$,$y$) is summed from $z = -h/2$ to $z = h/2$, and divided by h, where h is the fuel height (368 cm). These values are multiplied by the gamma radiation intensity (emitted photons per second per fuel assembly), tabulated in Table A2-1 to Table A2-3, times the number of assemblies per canister, to get the volumetric heat generation distribution at canister midplane. For a slab at an arbitrary height at $z^*$, the energy data values for each coordinate pair ($x$,$y$) should be summed from $z = z^* - h/2$ to $z = z^* + h/2$ instead. It is hereby implicitly assumed that all slabs are emitting and depositing photons equal to the slab at $z = 0$, which will make energy summations for slabs at other heights than z = 0 less realistic due to increasing influence from the canister ends modelled in the gamma ray simulations. The calculation methodology is further described and exemplified in Appendix 3.

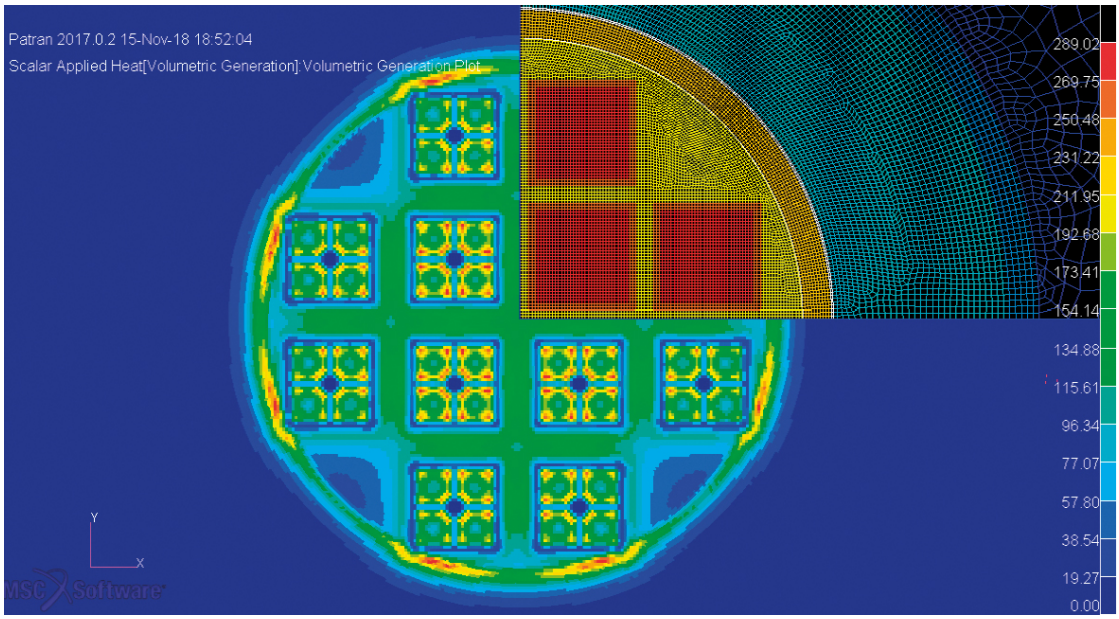


***Figure 2-4.*** *SVEA96S – volumetric heat generation (W/m³) from deposited gamma radiation at the canister's midplane 30 years after service.*

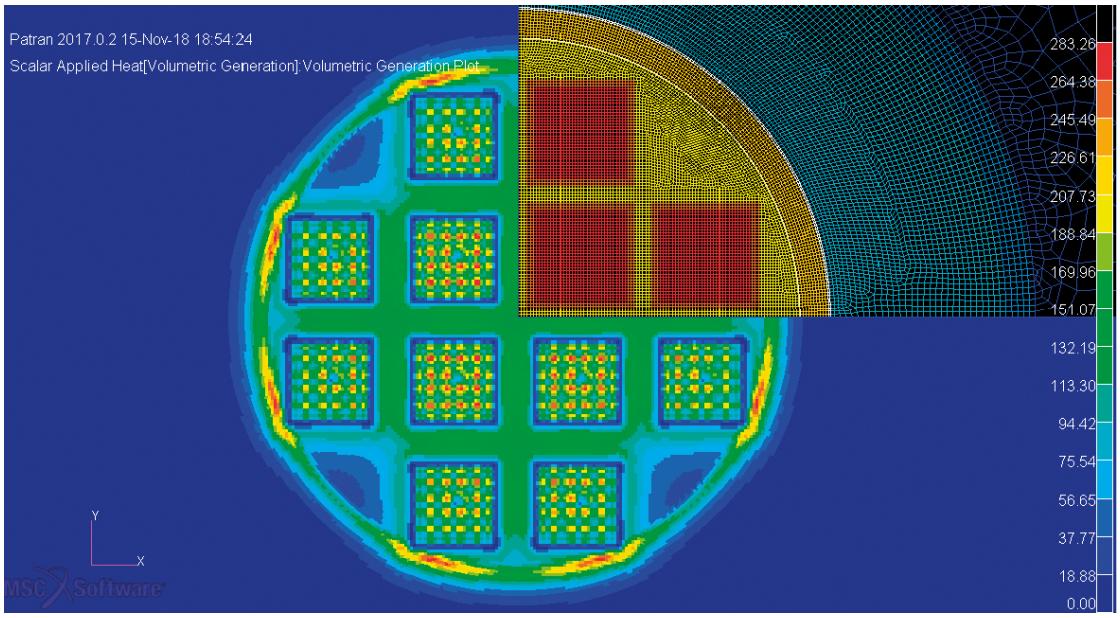


***Figure 2-5.*** *BWR8x8 – volumetric heat generation (W/m³) from deposited gamma radiation at the canister's midplane 30 years after service.*

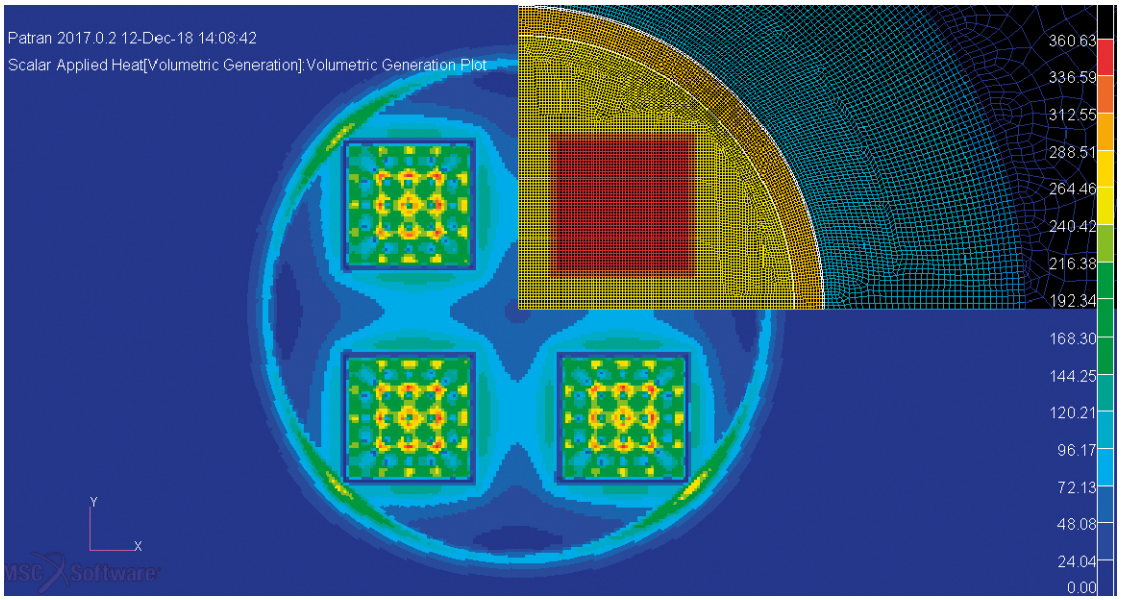


***Figure 2-6.*** *PWR17x17 – volumetric heat generation (W/m³) from deposited gamma radiation at the canister's midplane 30 years after service.*

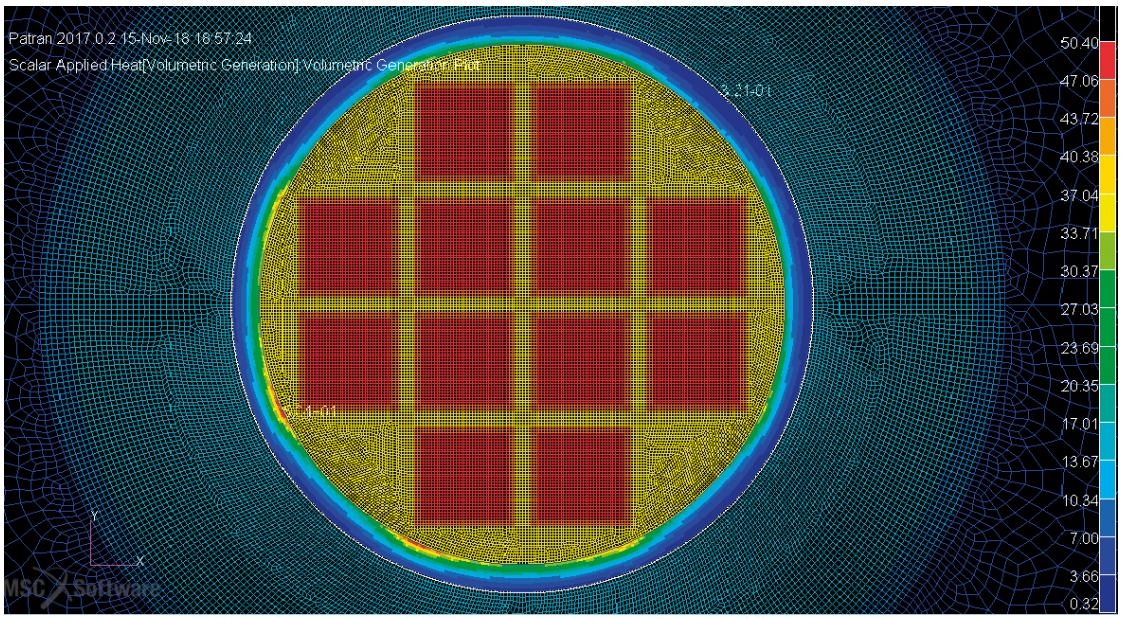


***Figure 2-7.*** *SVEA96S – volumetric heat generation (W/m³) from deposited gamma radiation in copper shell at the canister's midplane 30 years after service.*

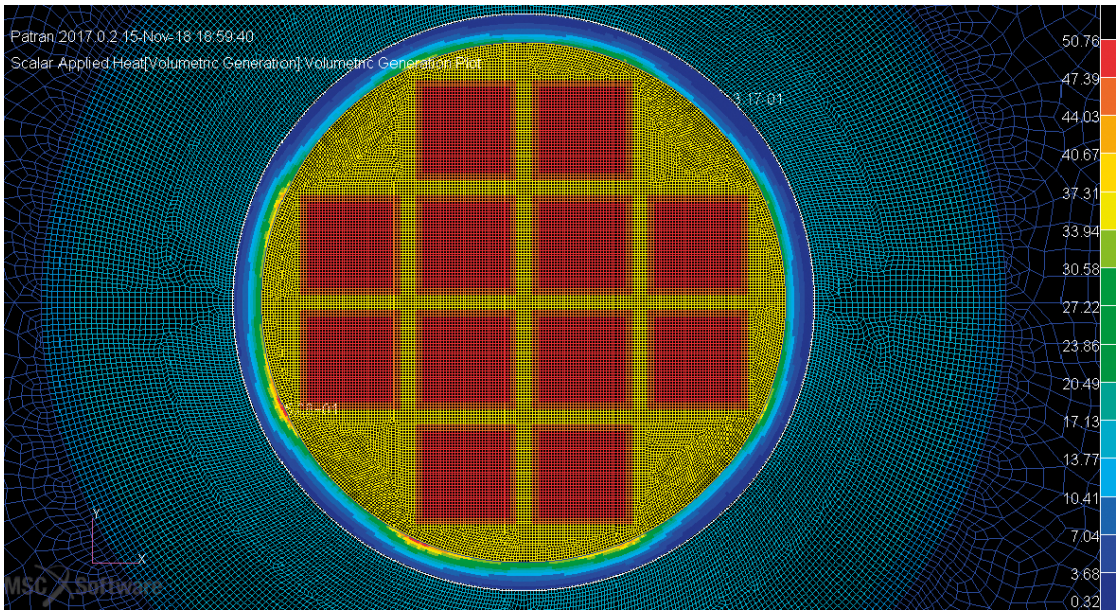


***Figure 2-8.*** *BWR8x8 – volumetric heat generation (W/m³) from deposited gamma radiation in copper shell at the canister's midplane 30 years after service.*

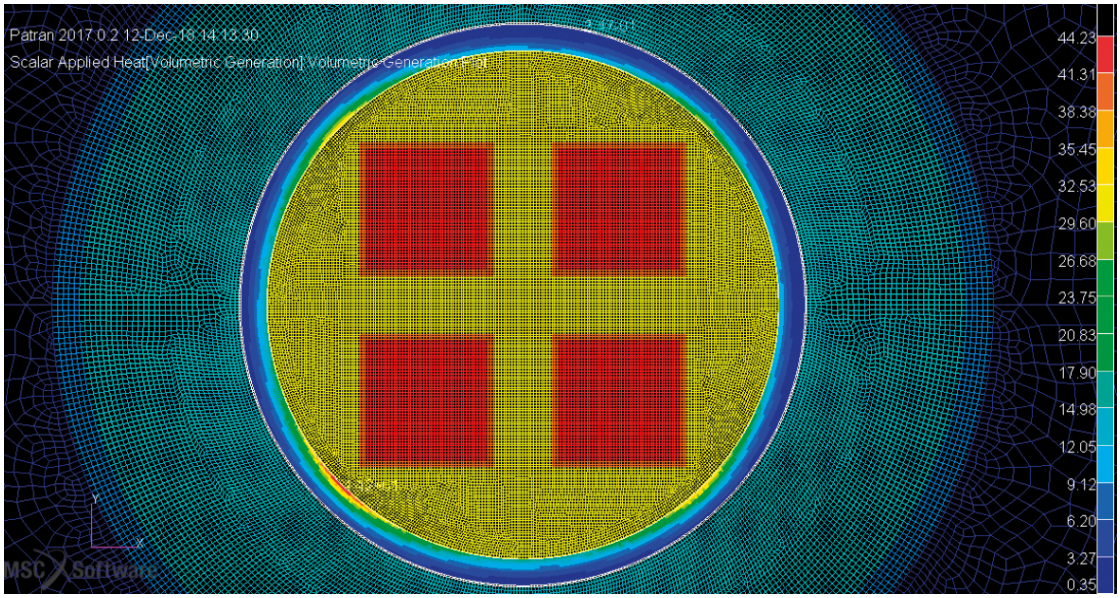


***Figure 2-9.*** *PWR17x17 – volumetric heat generation (W/m³) from deposited gamma radiation in copper shell at the canister's midplane 30 years after service.*

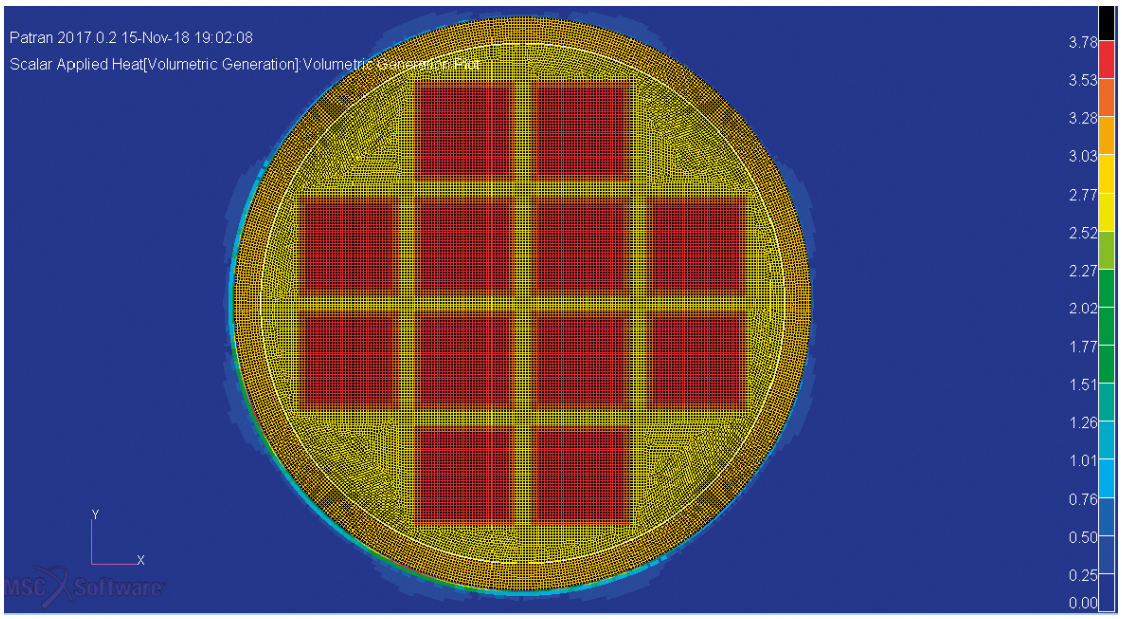


***Figure 2-10.*** *SVEA96S – volumetric heat generation (W/m³) from deposited gamma radiation in buffer and rock at the canister's midplane 30 years after service.*

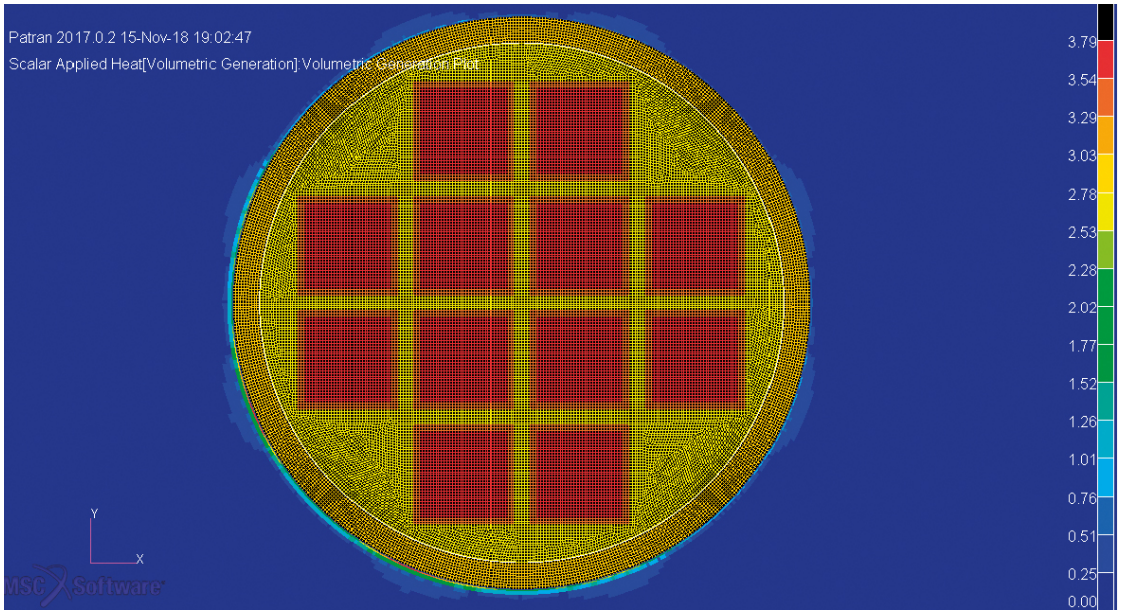


***Figure 2-11.*** *BWR8x8 – volumetric heat generation (W/m³) from deposited gamma radiation in buffer and rock at the canister's midplane 30 years after service.*

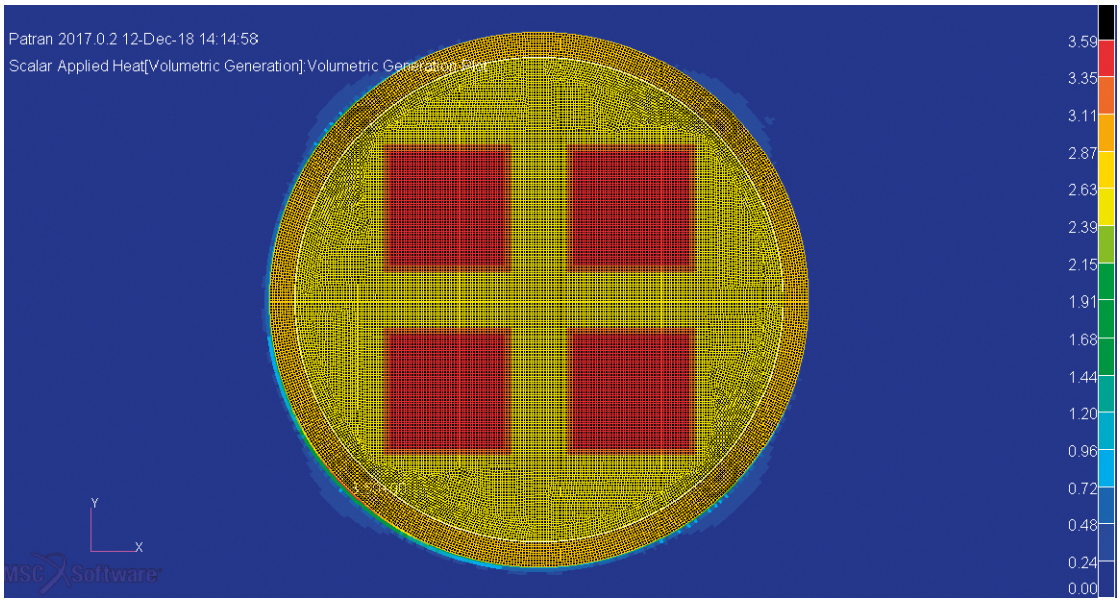


***Figure 2-12.*** *PWR17x17 – volumetric heat generation (W/m³) from deposited gamma radiation in buffer and rock at the canister's midplane 30 years after service.*

# 3 Thermal analysis model

## 3.1 General description

As described in Chapter 2 the results from the gamma ray simulations are most accurate close to the canister's midplane. Furthermore, it is shown in Ikonen (2017, Figures 61 and 63) that the temperature variation on and exterior of the copper shell – where our current focus is – is small, especially in the circumferential direction where the temperature varies by approximately 0.33 °C for an SKB-PWR canister even if the canister has different fuel assembly decay heat powers of 800 W, 300 W, 300 W and 300 W. These two facts together with an ambition to make a model simple enough for quick comparative analyses with maintained control motivate the choice of a one-dimensional, radial analysis model.

## 3.2 Geometry

Close to a single canister, near its midplane, the axial heat flux is low and the thermal conditions can be approximated by a cylindrical heat source (Hökmark et al. 2009). Far from the canister, in contrast, the conditions can be seen as a point heat source with a spherical thermal field.

Based on the above approach a one-dimensional, radial, thermal finite element model (FE-model) is built in the commercial programs MSC.Patran (pre- and post-processor) and MSC.Nastran (solver), see Figure 3-1, Figure 3-2 and Figure 3-3. The analysis model is chosen as a 1 cm thick (axial direction), 1 degree wide (circumferential derection) "piece of cake" located at the canister's midplane, which at a certain radial distance from the canister turns into a spherical piece, still 1 degree wide in the circumferential direction. The distance at which the transition from cylindrical to spherical geometry occurs is by trial calculations carefully chosen at 3 600 mm, which, as shown in Figure 3-4 and Figure 4-1, gives approximately the same thermal resistance as the axisymmetric model of a single Posiva-BWR canister presented by Ikonen (2017, p 58), expressed as the transient temperature on the copper shell surface. In the swedish report by Renström (2020, Appendix 3), a more natural way to choose the transition radius is discussed.

It is judged that BWR canisters and inserts from Posiva and SKB have sufficiently similar dimensions for the current comparative analyses to be relevant.

The in- and outside gaps at the copper shell are, as in Ikonen (2017), chosen at 1.5 mm and 10 mm respectively. As a reference, the largest possible internal and external radial gaps for concentrically placed inserts, canisters and buffer blocks are 1.75 and 11.1 mm, respectively, according to the design conditions (SKB 2010a, pp 29–34, 2010b, p 28). At a minimum, the internal gap at concentric positioning may be 1 mm. The external gap may be 8.9 mm for dry buffer blocks and 0 mm for wet.

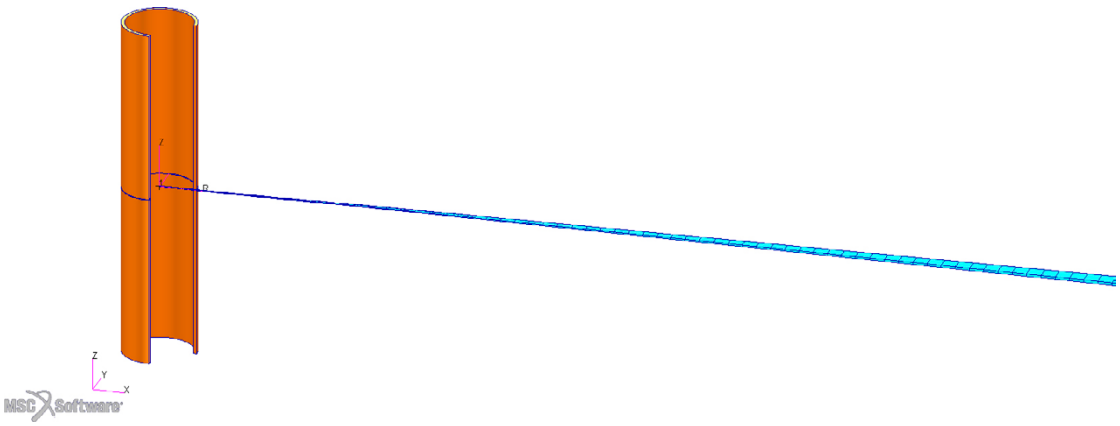


***Figure 3-1.*** *Thermal FE-model. The copper shell is shown as a reference. Blue = rock.*

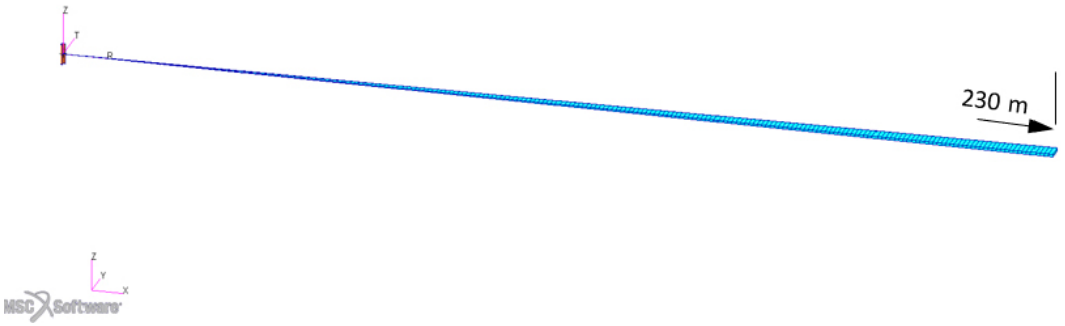


***Figure 3-2.*** *Thermal FE-model, overview. The copper shell is shown as a reference. Blue = rock.*

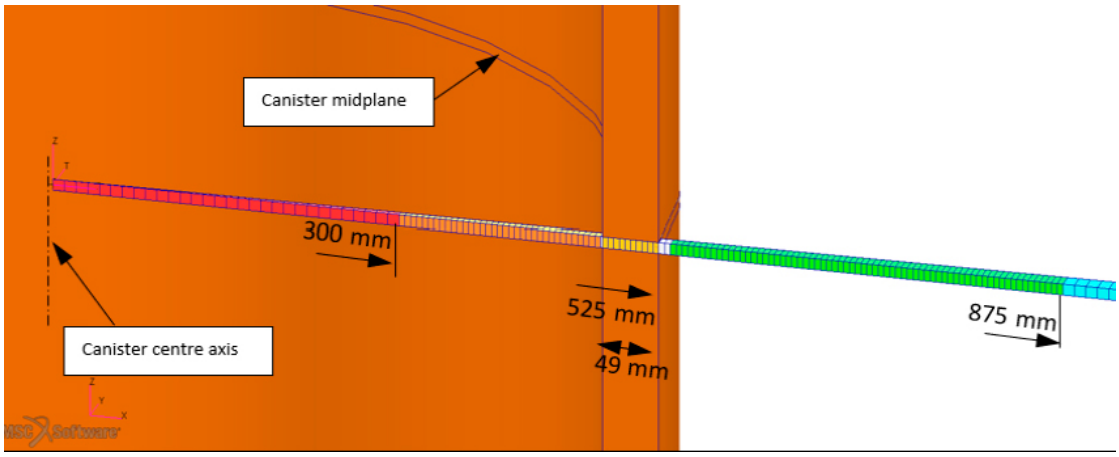


***Figure 3-3.*** *Thermal FE-model, detail at the canister. Red = canister internals with heat load, orange = canister internals without heat load, yellow = copper shell, green = buffer, blue = rock, white = inner and outer gap at copper shell, brown = copper shell shown as a reference.*

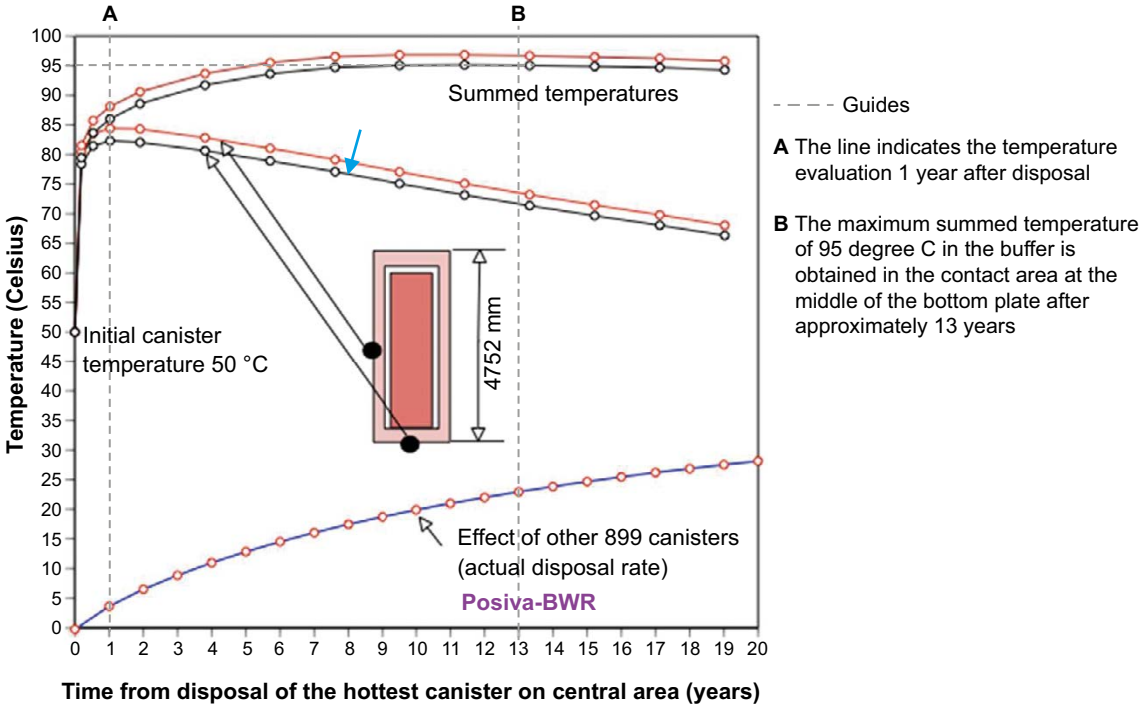


***Figure 3-4.*** *Temperature on the canister's copper surface from Ikonen (2017, Figure 52). Blue arrow = reference curve to be compared with the temperature curve for Load Case 1 in Figure 4-1.*

## 3.3 Material properties

Due to the model's one-dimensional nature the canister's internals cannot be modelled in detail. Therefore, the properties for fuel assemblies, tubes and insert are averaged according to Ikonen (2017, p 61).

The pellet-filled gap between the pre-compacted buffer blocks and rock is assumed to have the same properties as the buffer blocks, without gaps between them.

Heat is assumed to be transferred by conduction and radiation[2] only without phase changes. Convection effects in gas-filled gaps are, based on Ikonen (2017, Chapter 7.5), neglected.

Material properties are shown in Table 3-1. They are assumed at about 100 °C and are not considered temperature dependent. Short references are made to 1) Ikonen (2017), 2) Incropera et al. (2006), 3) Hökmark et al. (2010), 4) Ikonen (2009).

**Table 3-1. Material properties.**

| Material | k (W/m/K) | Ref. | $\rho \cdot c_p$ (MJ/m$^3$/K) | Ref. | ε (emissivity) | Ref. |
|---|---|---|---|---|---|---|
| Internals[3] | 23.6 | 1) | 2.7 | 1) | - | - |
| Nodular iron | - | - | - | - | 0.6 | 1) |
| Argon | 0.022 | 1) | 8.58E−04 | 1) | - | - |
| Copper | 390 | 1) | 3.45 | 1) | 0.1/0.3 in-/outside | 1) |
| Air | 0.03 | 1) | 8.8E−04 | 2) | - | - |
| Buffer | 1 | 3) | 2.4 | 1) | 0.8 | 4) |
| Rock | 2.55 | 1) 3) | 2.12 | 3) | - | - |

## 3.4 Boundary conditions

All boundaries are adiabatic in the FE-model, that is the heat flux is zero across all of them.

The initial temperature is assumed to be uniform at 50 °C at the canister and its internals (Ikonen 2017, Figure 52). Exterior of the canister, the initial temperature is assumed to be uniform at 11.2 °C (Ikonen 2017, p 59, Hökmark et al. 2010).

## 3.5 Thermal loads

### 3.5.1 Conventional method – Deposited gamma radiation not taken into account

In Ikonen (2017, p 61) the decay heat load is assumed to be uniformly distributed within a cylinder of radius 0.3 m. The same assumption is made in the current FE-model (Figure 3-3), with a chosen cylinder length of 3.68 m. Thus, when gamma ray simulations are not taken into account, all decay heat load is assumed to be located there.

The decay heat power for fuel with burn-up 40 MWd/kgU is taken from Ikonen (2017, Table 6) as shown in Table 3-2 with the assumption that one SKB-BWR canister contains 2 100 kg Uranium (Ikonen 2017, Table 6), for instance 1 340 (W/tU) · 2.1(tons) = 2 814 (W). The decay power value for 33 years after service is interpolated to about 1 705 W which is chosen as initial value in the thermal analysis. It has been judged that it is of interest to study and compare canisters with an initial total decay heat load at about 1 700 W at final repository deposition, since this value has been used in several analyses before, for instance, Hökmark et al. (2009) and Ikonen (2017).

[2] According to Stefan-Boltzmann's law.

[3] Averaged properties for fuel, zirconium, argon, steel and nodular iron.

**Table 3-2. Decay heat power.**

| Years after service | SKB-BWR (W/tU) | Per canister (W) |
|---|---|---|
| 10 | 1 340 | 2 814 |
| 20 | 1 040 | 2 184 |
| 30 | 854 | 1 793.4 |
| 33 = the time of deposition, t = 0 in thermal analyses | 812 | 1 705.2 |
| 40 | 714 | 1 499.4 |
| 50 | 603 | 1 266.3 |
| 60 | 514 | 1 079.4 |
| 70 | 443 | 930.3 |
| 80 | 386 | 810.6 |
| 90 | 340 | 714 |
| 100 | 303 | 636.3 |

Because the finite element model is simplified and does not comprise a complete canister, some further assumptions have to be made about how to apply the 1 705 W initial heat load ($Q$). It has been chosen to focus on realistic values of the radial heat flux through the outer copper surface since this region is of our main interest. According to Hökmark et al. (2009, p 27), an estimate of the local heat flux through the copper surface at canister midplane is about 87 % of the average heat flux for the whole canister, defined as the factor $\Phi = 0.87$. Therefore, the initial decay heat power load per volume in the red region in Figure 3-3 is chosen as follows:

If Q were uniformly distributed over the loaded volume, the heat power load per volume would be

$1\,705\ \text{W}/(\pi \cdot (0.3\ \text{m})^2 \cdot 3.68\ \text{m}) = 1\,639\ \text{W/m}^3$

which in the finite element model, with radial heat transfer only, would give a heat flux over the copper surface of

$1\,705\ \text{W}/(2 \cdot \pi \cdot 0.525\ \text{m} \cdot 3.68\ \text{m}) = 140.5\ \text{W/m}^2$

However, the average heat flux over the whole canister is

$1\,705\ \text{W}/(2 \cdot \pi \cdot 0.525\ \text{m} \cdot (0.525\ \text{m} + 4.83\ \text{m})) = 96.5\ \text{W/m}^2$

and, with $\Phi = 0.87$, a realistic value locally at canister midplane should be

$96.5\ \text{W/m}^2 \cdot 0.87 = 84.0\ \text{W/m}^2$

Since

$84.0\ \text{W/m}^2 / 140.5\ \text{W/m}^2 = 0.60$

the applied initial decay heat power load per volume in the red region in Figure 3-3 is adjusted and chosen at

$0.60 \cdot 1\,639\ \text{W/m}^3 = 983.4\ \text{W/m}^3$

### 3.5.2 Comparative method – Deposited gamma radiation taken into account

As a comparison to the conventional thermal loading method, heat power from the deposited gamma radiation is taken into account by using the results from the gamma ray simulation of SVEA96S (Figure 2-4, Figure 2-7 and Figure 2-10). The calculated deposited gamma power from Cs-137 and Eu-154 after 30 years' cooling time is 294.9 W which should be about 24 % of the total residual heat power (Table 2-2). With the power values in Table 3-2, 294.9 W is only (294.9W/1 793.4W) = 16.4 % of the total residual heat power which most likely would be an under-estimation. This is to a high degree compensated for in the analysis model thanks to our adjustment of total residual heat to realistic heat flux described in Section 3.5.1: in terms of heat flux, a more realistic relation of

$$(294.9\ \text{W}/(1\,793.4\ \text{W} \cdot 0.6)) = 27\ \%$$

is reached between deposited gamma radiation power and total residual heat power.

Since the analysis model is geometrically one-dimensional, it obviously needs a one-dimensional heat load. Therefore, the deposited gamma radiation power of SVEA96S shown in Figure 2-4, Figure 2-7 and Figure 2-10 is averaged over 360° for each radius, as shown in Figure 3-5. From this, the gamma radiation power depositied outside the canister is calculated to about 0.5 W.

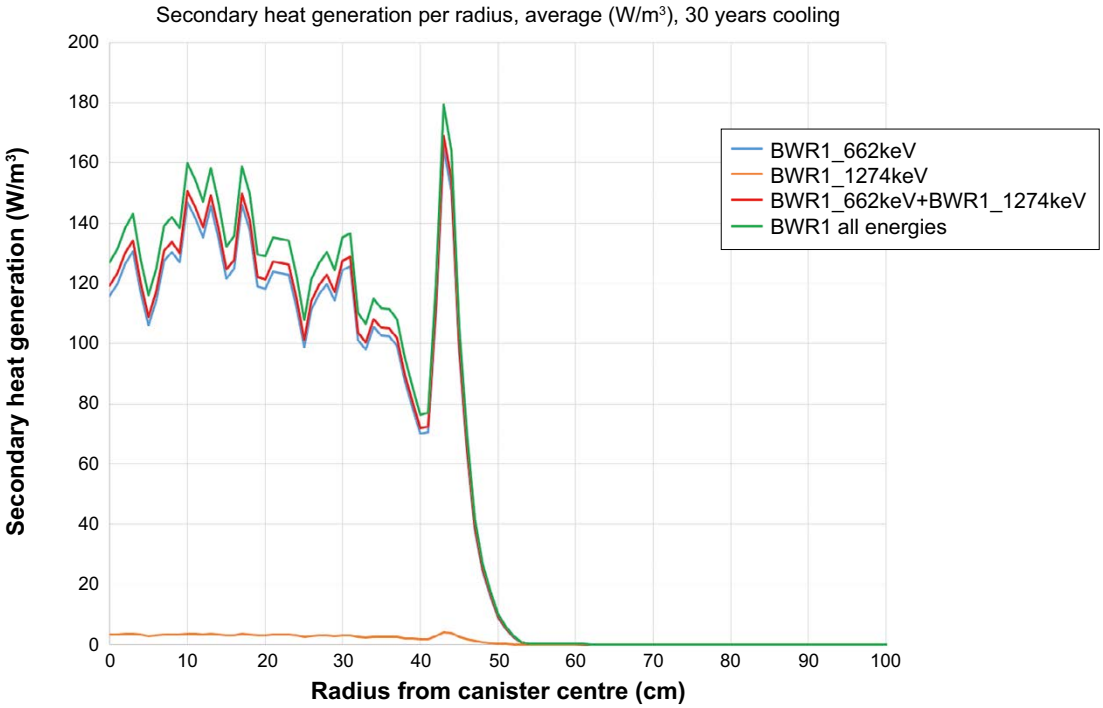


***Figure 3-5.*** *Deposited gamma radiation power of SVEA96S averaged over 360° for each radius. The contribution from Cs-137 in blue, from Eu-154 in orange, the sum of Cs-137 and Eu-154, which is used as deposited gamma power load in Chapter 3.6, in red, the total gamma power emission in green. The total gamma power emission is approximated by summing the gamma power for all energy levels, assuming that deposition of gamma emission at 0 to 0.9 MeV has the same spatial distribution as Cs-137 whereas gamma emission at 0.9 to 12 MeV has the same distribution as Eu-154. The gamma power part emitted by Cs-137 and Eu-154 is estimated to represent about 95 % of the total gamma power emission as shown in Chapter 2.2.*

## 3.6 Load cases

Five load cases are defined, of which the first has the residual heat uniformly and entirely generated inside radius 300 mm as described in Section 3.5.1, similar to Ikonen (2017). The second Load Case has 27 % of the residual heat generated by Cs-137 and Eu-154 according to Section 3.5.2 and the red line in Figure 3-5, simulating deposited gamma power, whereas the rest of the residual heat, 73 %, is generated in the conventional way as in Load Case 1. Load Case 3, 4 and 5 should be seen as comparative sensitivity analyses, in which 27 % of the residual heat is generated in the copper shell, a narrow torus of buffer and the whole buffer, respectively (Table 3-3).

**Table 3-3. Load cases. Load A = part of residual heat load generated inside radius 300 mm, Load B = part of residual heat load emanating from deposited gamma radiation.**

| Load Case no | Load A | Load B | Load B distribution | Load B location |
|---|---|---|---|---|
| 1 | 100 % | 0 % | - | - |
| 2 | 73 % | 27 % | red line in Figure 3-5 | red line in Figure 3-5 |
| 3 | 73 % | 27 % | uniform | in copper shell only |
| 4 | 73 % | 27 % | uniform | in 50 mm inner torus of buffer only |
| 5 | 73 % | 27 % | uniform | in buffer only |

# 4 Results

The surface temperature at the midplane of a single canister with the residual heat load modelled according to the conventional method as described in Section 3.5.1, from the time of deposition in the final repository to 20 years after deposition, is shown as Load Case 1 in Figure 4-1. It agrees well with results from Ikonen (2017) as shown in Figure 3-4, as expected, since the analysis model is adjusted to fit these results. The surface temperature calculated for Load Case 1 is in Figure 4-1 compared to results from Load Case 2 to 5 in which the heat load from deposited gamma radiation is modelled as described in Section 3.6.

In Figure 4-2 to Figure 4-5 the calculated temperature at midplane for a single canister as a function of radial distance from the centre axis is shown for Load Case 1 to 5 at different times after deposition in the final repository. The calculated surface temperature at 0.5, 3 and 10 years after deposition is tabulated in Table 4-1.

**Table 4-1. Calculated surface temperature at the midplane for a single canister at different times after deposition in the final repository for Load Case 1 to 5.**

| Load Case no | 0.5 years | 3.0 years | 10 years | Maximum |
|---|---|---|---|---|
| 1 | 80.0 °C | 82.4 °C | 75.8 °C | 82.9 °C |
| 2 | 79.8 °C | 82.3 °C | 75.6 °C | 82.9 °C |
| 3 | 80.0 °C | 82.4 °C | 75.8 °C | 82.9 °C |
| 4 | 75.6 °C | 78.3 °C | 72.2 °C | 78.6 °C |
| 5 | 72.9 °C | 75.7 °C | 70.1 °C | 76.0 °C |

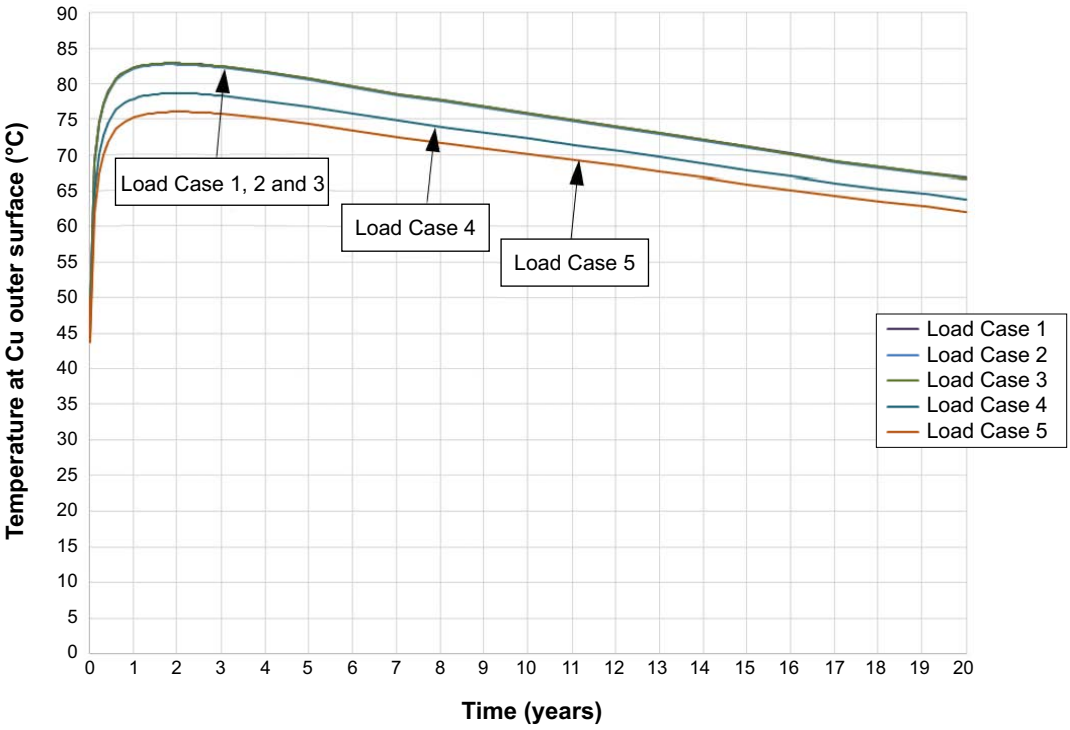


***Figure 4-1.*** *Surface temperature at midplane for a single canister for Load Case 1 to 5.*

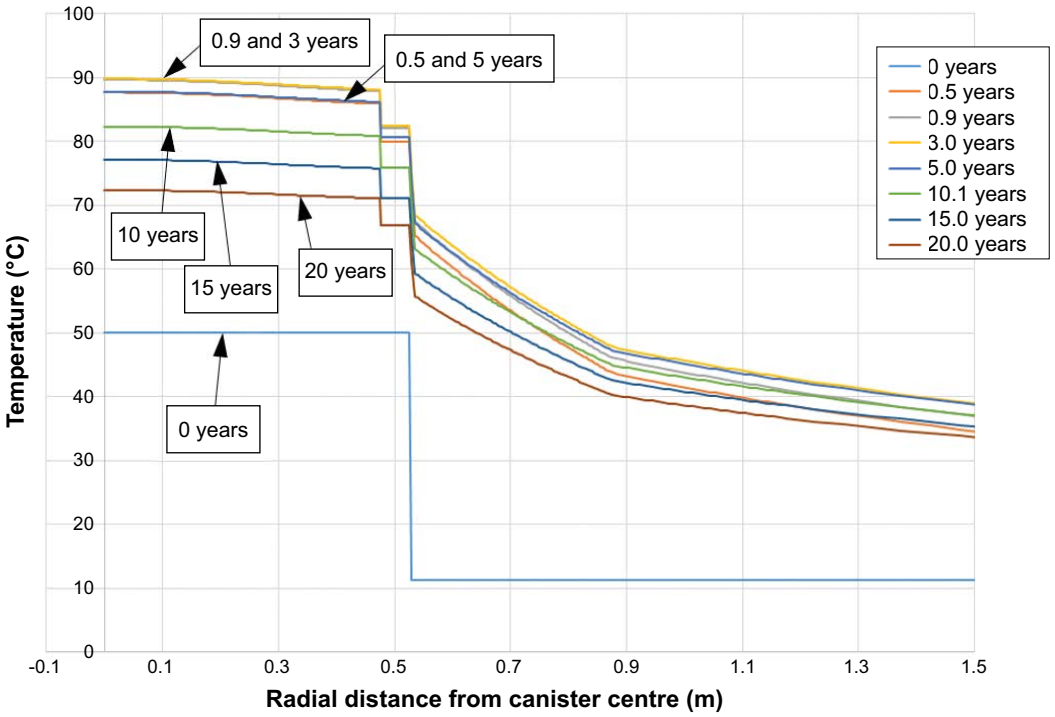


***Figure 4-2.*** *Calculated temperature at the midplane of a single canister as a function of radial distance from the centre axis for Load Case 1 at different times after deposition in the final repository.*

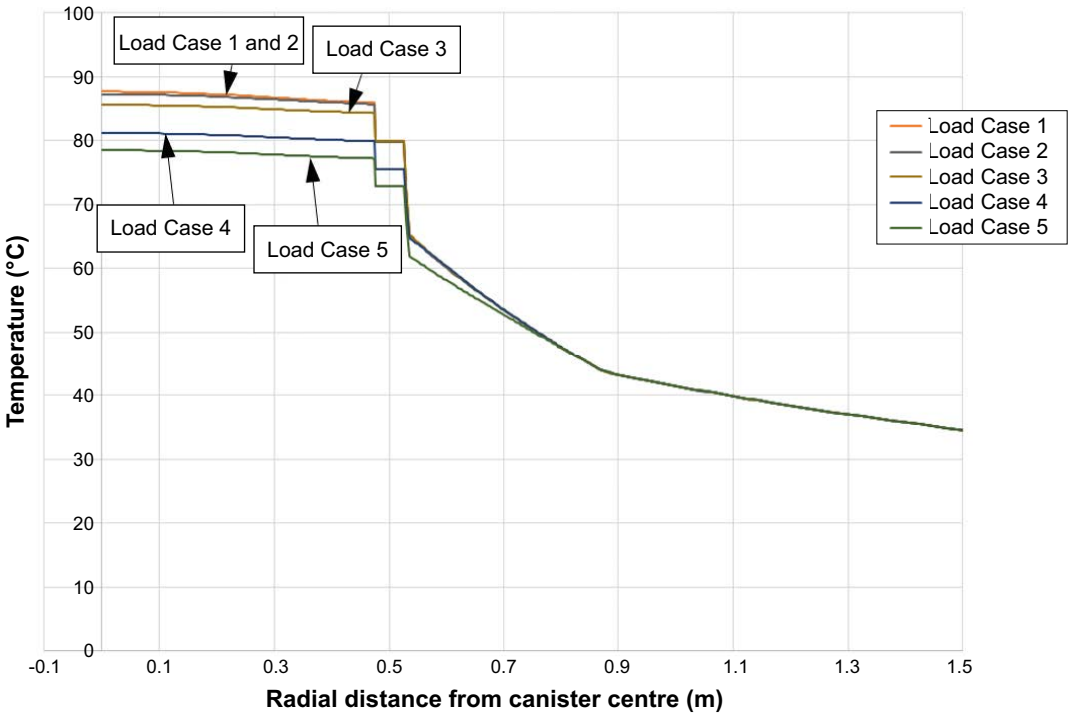


***Figure 4-3.*** *Calculated temperature at the midplane of a single canister as a function of radial distance from the centre axis for Load Case 1 to 5 at 0.5 years after deposition in the final repository.*

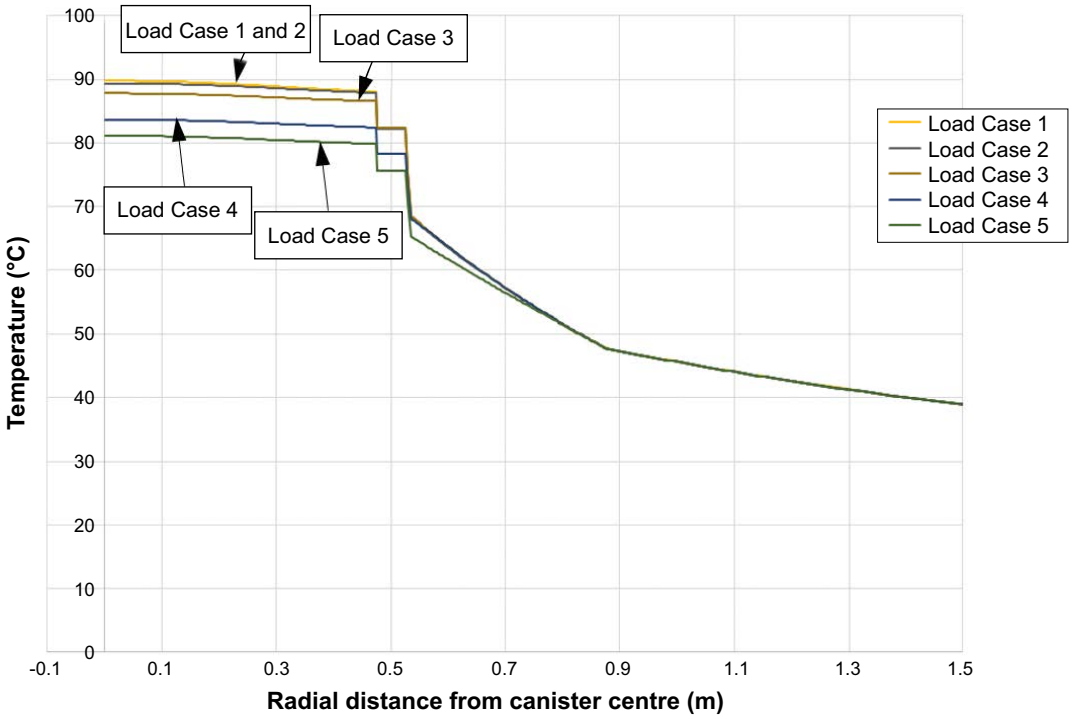


***Figure 4-4.*** *Calculated temperature at the midplane of a single canister as a function of radial distance from the centre axis for Load Case 1 to 5 at 3 years after deposition in the final repository.*

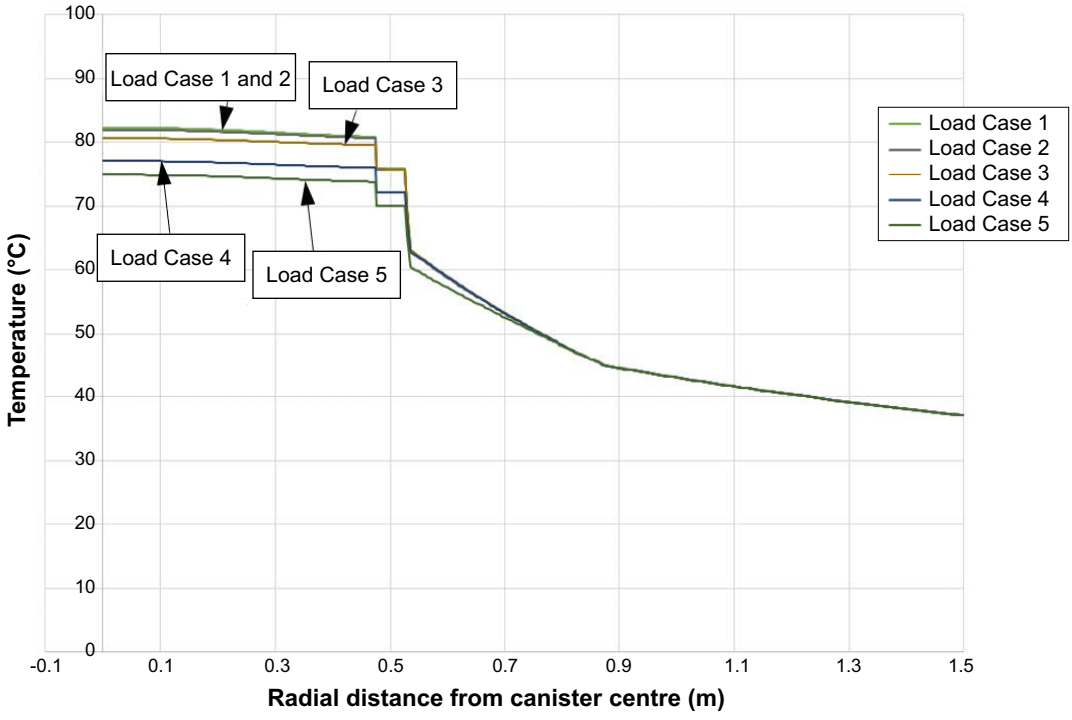


***Figure 4-5.*** *Calculated temperature at the midplane of a single canister as a function of radial distance from the centre axis for Load Case 1 to 5 at 10 years after deposition in the final repository.*

# 5 Conclusions

For the three different fuel configurations studied, SVEA96S, BWR8x8 and PWR17x17, the following can be concluded:

From Chapter 2.2 and Appendix 2:

- radiation from Cesium and Europium together covers at least 95 % of the emitted gamma energy for cooling times 30 years and longer.

Furthermore, with the assumption that radiation from Cs and Eu covers a representative amount of the total emitted energy from gamma radiation at all levels, the following can be concluded:

From Figure 3-5:

- at the studied part of the canister, the midplane slab of 1 cm thickness, the amount of gamma energy deposited outside the canister is less than 0.2 % of the amount deposited inside the canister,
- the heat power from emitted gamma energy deposited outside the canister is small compared to the heat generation inside the canister.

From Figure 4-1 and Table 4-1:

- calculations of the temperature on and exterior of the copper shell made with the conventional model simplifications, in this case with the residual heat uniformly and entirely generated inside a radius of 300 mm, gives virtually the same results as if the spatial distribution of deposited energy from gamma radiation were taken into account,
- a model with all the deposited energy from gamma radiation hypothetically located in the copper shell still gives virtually the same temperature on and exterior of the copper shell as the conventional model,
- a model with all the deposited energy from gamma radiation hypothetically located in the buffer would give a few degrees lower temperature on and exterior of the copper shell compared to the conventional model,
- the spatial distribution of deposited energy from gamma radiation does not affect the temperature on and exterior of the copper shell unless a significant amount of energy is deposited outside the canister,
- it is not necessary to take the spatial distribution of deposited energy from gamma radiation into account when calculating the temperature on and exterior of the copper shell.

# 6 Discussion

The current study focuses on the temperature development at the copper shell and the buffer at the midplane of a single canister. As shown in Chapter 3, the chosen one-dimensional radial analysis model should be a reasonable approximation for this. Since only a very small amount of gamma energy is deposited outside the canister, its influence on temperature development at and outside the shell can be disregarded. On the other hand, in a temperature study of the canister internals, the spatial distribution of deposited gamma energy, as shown in Figure 2-4 to Figure 2-12, might be of significant importance.

The thermal calculations have been made for one type of fuel only, namely SVEA96S with 33 years of cooling time after service. Considering that the two other fuel types, BWR8x8 and PWR17x17, have almost identical gamma radiation intensities (Figure 2-2), calculations for them most likely would yield the same conclusions. Fuel with shorter cooling time generally has a higher degree of photons with high kinetic energy, which means that a somewhat larger part of the total decay energy could be deposited outside the canister if such a fuel is encapsulated. However, emissions from Cs-137 are still dominant at shorter cooling times, at least longer than ten years. Therefore, the conclusions are considered valid for fuels of the studied type with cooling times longer than 10 years.

For the local temperature development at the canister, other parameters than the spatial distribution of deposited gamma energy, such as sizes of air- or water-filled gaps, buffer cracks, buffer water contents and material properties of buffer and rock, should be of much higher importance. Sensitivity studies of this kind of parameters could be performed in the current analysis model, or, even more easily, in handbook based analytical steady-state calculations, since the temperature field at the copper shell and buffer approximately is quasi-stationary in a time-scale from one year to another.

Quasi-stationary conditions can be shown by studying the Fourier Number $Fo = k \cdot t/\rho c_p L^2$, which is a dimensionless number measuring the importance of heat transfer related to heat storage capacity in a physical problem, that is Fo>>1 => stationary conditions whereas Fo << 1 => transient conditions. For the canister, $Fo \approx 23.6 \cdot t/(2.7E6 \cdot 1^2) = 8.7e{-}6 \cdot t$ and for the buffer $Fo \approx 1 \cdot t/(2.4E6 \cdot 1^2) = 4.2E{-}7 \cdot t$, which for Fo = 1, that is, equal importance of heat transfer and heat storage, gives t = 1/8.7E−6 s = 1.3 days for the canister and t = 1/4.2E−7 s = 27.5 days for the buffer. Thus, for time spans significantly longer than a month, the temperature field close to the canister can be regarded as quasi-stationary.

In studies of thermal interaction between several canisters in the final repository, such as distance optimization, where the physical model length scale is an order of magnitude higher than that in the current study, the effect of spatial distribution of deposited gamma energy definitely could be neglected.

# References

SKB's (Svensk Kärnbränslehantering AB) publications can be found at www.skb.com/publications. SKBdoc documents will be submitted upon request to document@skb.se.

**Hökmark H, Lönnqvist M, Kristensson O, Sundberg J, Hellström G, 2009.** Strategy for thermal dimensioning of the final repository for spent nuclear fuel. SKB R-09-04, Svensk Kärnbränslehantering AB.

**Hökmark H, Lönnqvist M, Fälth B, 2010.** THM-issues in repository rock. Thermal, mechanical, thermo-mechanical and hydro-mechanical evolution of the rock at the Forsmark and Laxemar sites. SKB TR-10-23, Svensk Kärnbränslehantering AB.

**Ikonen K, 2009.** Thermal dimensioning of spent fuel repository. Posiva Working Report 2009-69, Posiva Oy, Finland.

**Ikonen K, 2017.** Temperatures inside SKB and Posiva type disposal canisters for spent fuel. Posiva Oy. SKBdoc 1495080 ver 1.0, Svensk Kärnbränslehantering AB.

**Incropera F P, DeWitt D, Bergman T L, Lavine A S, 2006.** Fundamentals of heat and mass transfer. 6th ed. New York: Wiley.

**Jansson P, 2002.** Studies of nuclear fuel by means of nuclear spectroscopic methods. PhD thesis. Uppsala University, Sweden.

**Renström P, 2020.** Beräkningar av temperaturen i kopparhöljet och bufferten i förenklade parameterstudier. SKB R-19-27, Svensk Kärnbränslehantering AB. (In Swedish.)

**SKB, 2010a.** Design, production and initial state of the canister. SKB TR-10-14, Svensk Kärnbränslehantering AB.

**SKB, 2010b.** Design, production and initial state of the buffer. SKB TR-10-15, Svensk Kärnbränslehantering AB.

# Appendix 1

## Data files

Data from gamma ray simulations:

BWR1_1274keV.csv
BWR1_662keV.csv
BWR6_1274keV.csv
BWR6_662keV.csv
PWR8_1274keV.csv
PWR8_662keV.csv

# Appendix 2

## Gamma radiation intensities

Gamma radiation intensities (number of photons emitted per fuel assembly per second) from SKB's Nuclide Database are tabulated in Table A2-1, Table A2-2 and Table A2-3 below.

**Table A2-1. Gamma radiation intensities for SVEA-96S.**

| Burnup | 40 | | | | | | |
|---|---|---|---|---|---|---|---|
| Power | 4 | | | | | | |
| Case | Kons | | | | | | |
| DecayTime | 10 | 20 | 30 | 40 | 50 | 60 | 70 |
| Spectraend | Summa | | | | | | |
| 0.02 | 2.16E+12 | 1.68E+12 | 1.35E+12 | 1.09E+12 | 8.91E+11 | 7.32E+11 | 6.06E+11 |
| 0.03 | 1.93E+12 | 1.41E+12 | 1.11E+12 | 8.76E+11 | 6.95E+11 | 5.53E+11 | 4.42E+11 |
| 0.045 | 3.84E+12 | 2.85E+12 | 2.20E+12 | 1.72E+12 | 1.35E+12 | 1.06E+12 | 8.34E+11 |
| 0.06 | 2.47E+12 | 2.03E+12 | 1.72E+12 | 1.47E+12 | 1.27E+12 | 1.11E+12 | 9.80E+11 |
| 0.07 | 1.27E+12 | 9.63E+11 | 7.51E+11 | 5.86E+11 | 4.59E+11 | 3.59E+11 | 2.81E+11 |
| 0.075 | 6.15E+11 | 4.69E+11 | 3.68E+11 | 2.90E+11 | 2.29E+11 | 1.81E+11 | 1.44E+11 |
| 0.1 | 2.98E+12 | 2.19E+12 | 1.69E+12 | 1.31E+12 | 1.03E+12 | 8.04E+11 | 6.30E+11 |
| 0.15 | 5.19E+12 | 3.56E+12 | 2.61E+12 | 1.98E+12 | 1.52E+12 | 1.18E+12 | 9.20E+11 |
| 0.2 | 3.77E+12 | 2.82E+12 | 2.20E+12 | 1.71E+12 | 1.34E+12 | 1.05E+12 | 8.19E+11 |
| 0.26 | 2.93E+12 | 2.12E+12 | 1.60E+12 | 1.23E+12 | 9.55E+11 | 7.44E+11 | 5.81E+11 |
| 0.3 | 1.49E+12 | 1.14E+12 | 8.88E+11 | 6.95E+11 | 5.45E+11 | 4.28E+11 | 3.37E+11 |
| 0.4 | 4.09E+12 | 3.08E+12 | 2.40E+12 | 1.87E+12 | 1.46E+12 | 1.14E+12 | 8.95E+11 |
| 0.45 | 2.15E+12 | 1.17E+12 | 8.71E+11 | 6.74E+11 | 5.25E+11 | 4.10E+11 | 3.21E+11 |
| 0.51 | 2.15E+12 | 1.24E+12 | 9.44E+11 | 7.34E+11 | 5.73E+11 | 4.47E+11 | 3.49E+11 |
| 0.512 | 5.46E+11 | 2.39E+10 | 1.21E+10 | 6.30E+09 | 3.28E+09 | 1.71E+09 | 8.91E+08 |
| 0.6 | 7.47E+12 | 1.16E+12 | 6.34E+11 | 4.39E+11 | 3.20E+11 | 2.40E+11 | 1.83E+11 |
| 0.7 | 3.88E+14 | 2.88E+14 | 2.28E+14 | 1.81E+14 | 1.43E+14 | 1.14E+14 | 9.03E+13 |
| 0.8 | 3.45E+13 | 3.39E+12 | 1.35E+12 | 7.89E+11 | 5.11E+11 | 3.52E+11 | 2.55E+11 |
| 0.9 | 4.55E+12 | 1.65E+12 | 9.10E+11 | 5.56E+11 | 3.66E+11 | 2.55E+11 | 1.86E+11 |
| 1 | 4.56E+12 | 2.21E+12 | 1.13E+12 | 6.15E+11 | 3.61E+11 | 2.29E+11 | 1.56E+11 |
| 1.2 | 4.14E+12 | 1.47E+12 | 8.19E+11 | 5.06E+11 | 3.35E+11 | 2.36E+11 | 1.72E+11 |
| 1.33 | 9.57E+12 | 4.36E+12 | 2.02E+12 | 9.61E+11 | 4.75E+11 | 2.48E+11 | 1.39E+11 |
| 1.44 | 1.88E+12 | 1.60E+11 | 7.70E+10 | 5.72E+10 | 4.40E+10 | 3.40E+10 | 2.64E+10 |
| 1.5 | 2.42E+11 | 1.16E+11 | 6.17E+10 | 3.53E+10 | 2.18E+10 | 1.44E+10 | 1.01E+10 |
| 1.57 | 7.30E+10 | 3.80E+10 | 2.68E+10 | 1.96E+10 | 1.48E+10 | 1.13E+10 | 8.71E+09 |
| 1.66 | 9.59E+11 | 4.41E+11 | 2.09E+11 | 1.03E+11 | 5.34E+10 | 2.97E+10 | 1.78E+10 |
| 1.8 | 4.67E+10 | 2.77E+10 | 2.14E+10 | 1.66E+10 | 1.30E+10 | 1.01E+10 | 7.90E+09 |
| 2 | 3.02E+10 | 1.38E+10 | 1.07E+10 | 8.31E+09 | 6.48E+09 | 5.06E+09 | 3.95E+09 |
| 2.15 | 9.36E+09 | 2.54E+09 | 1.98E+09 | 1.55E+09 | 1.21E+09 | 9.48E+08 | 7.41E+08 |
| 2.35 | 1.92E+10 | 3.95E+07 | 2.49E+07 | 1.80E+07 | 1.31E+07 | 9.65E+06 | 7.18E+06 |
| 2.5 | 1.00E+10 | 2.20E+07 | 8.81E+06 | 6.87E+06 | 5.37E+06 | 4.20E+06 | 3.29E+06 |
| 2.75 | 1.60E+09 | 1.13E+08 | 1.00E+08 | 8.96E+07 | 8.03E+07 | 7.21E+07 | 6.49E+07 |
| 3 | 1.41E+09 | 1.02E+07 | 5.97E+06 | 4.15E+06 | 2.90E+06 | 2.06E+06 | 1.48E+06 |
| 3.5 | 3.61E+08 | 1.22E+07 | 8.18E+06 | 5.68E+06 | 3.98E+06 | 2.81E+06 | 2.02E+06 |
| 4 | 1.18E+07 | 7.92E+06 | 5.47E+06 | 3.80E+06 | 2.66E+06 | 1.88E+06 | 1.35E+06 |
| 4.5 | 7.57E+06 | 5.20E+06 | 3.59E+06 | 2.50E+06 | 1.75E+06 | 1.24E+06 | 8.87E+05 |
| 5 | 4.90E+06 | 3.37E+06 | 2.33E+06 | 1.62E+06 | 1.13E+06 | 8.00E+05 | 5.74E+05 |
| 5.5 | 3.14E+06 | 2.16E+06 | 1.49E+06 | 1.04E+06 | 7.25E+05 | 5.12E+05 | 3.68E+05 |
| 6 | 2.00E+06 | 1.37E+06 | 9.47E+05 | 6.58E+05 | 4.60E+05 | 3.25E+05 | 2.33E+05 |
| 6.5 | 1.26E+06 | 8.65E+05 | 5.97E+05 | 4.14E+05 | 2.90E+05 | 2.05E+05 | 1.47E+05 |
| 7 | 7.87E+05 | 5.41E+05 | 3.74E+05 | 2.60E+05 | 1.81E+05 | 1.28E+05 | 9.20E+04 |
| 7.5 | 4.90E+05 | 3.37E+05 | 2.33E+05 | 1.62E+05 | 1.13E+05 | 7.99E+04 | 5.73E+04 |
| 8 | 3.04E+05 | 2.09E+05 | 1.44E+05 | 1.00E+05 | 7.00E+04 | 4.95E+04 | 3.55E+04 |
| 10 | 4.17E+05 | 2.87E+05 | 1.98E+05 | 1.37E+05 | 9.60E+04 | 6.79E+04 | 4.87E+04 |
| 12 | 2.63E+04 | 1.81E+04 | 1.25E+04 | 8.68E+03 | 6.07E+03 | 4.29E+03 | 3.07E+03 |

**Table A2-2. Gamma radiation intensities for BWR 8x8.**

| Burnup | 38 | | | | | | |
|---|---|---|---|---|---|---|---|
| Power | 4 | | | | | | |
| Case | Kons | | | | | | |
| DecayTime | 10 | 20 | 30 | 40 | 50 | 60 | 70 |
| Spectraend | Summa | | | | | | |
| 0.02 | 2.17E+12 | 1.69E+12 | 1.36E+12 | 1.10E+12 | 8.96E+11 | 7.35E+11 | 6.07E+11 |
| 0.03 | 1.93E+12 | 1.43E+12 | 1.12E+12 | 8.87E+11 | 7.03E+11 | 5.59E+11 | 4.47E+11 |
| 0.045 | 3.82E+12 | 2.85E+12 | 2.21E+12 | 1.72E+12 | 1.35E+12 | 1.06E+12 | 8.37E+11 |
| 0.06 | 2.49E+12 | 2.04E+12 | 1.73E+12 | 1.47E+12 | 1.27E+12 | 1.11E+12 | 9.73E+11 |
| 0.07 | 1.28E+12 | 9.77E+11 | 7.62E+11 | 5.95E+11 | 4.65E+11 | 3.64E+11 | 2.85E+11 |
| 0.075 | 6.20E+11 | 4.74E+11 | 3.72E+11 | 2.92E+11 | 2.31E+11 | 1.83E+11 | 1.45E+11 |
| 0.1 | 3.00E+12 | 2.22E+12 | 1.71E+12 | 1.33E+12 | 1.04E+12 | 8.16E+11 | 6.39E+11 |
| 0.15 | 5.17E+12 | 3.58E+12 | 2.64E+12 | 2.00E+12 | 1.54E+12 | 1.19E+12 | 9.32E+11 |
| 0.2 | 3.81E+12 | 2.87E+12 | 2.23E+12 | 1.74E+12 | 1.36E+12 | 1.07E+12 | 8.33E+11 |
| 0.26 | 2.94E+12 | 2.14E+12 | 1.63E+12 | 1.25E+12 | 9.70E+11 | 7.56E+11 | 5.90E+11 |
| 0.3 | 1.51E+12 | 1.15E+12 | 9.02E+11 | 7.06E+11 | 5.54E+11 | 4.35E+11 | 3.41E+11 |
| 0.4 | 4.14E+12 | 3.13E+12 | 2.44E+12 | 1.91E+12 | 1.49E+12 | 1.17E+12 | 9.11E+11 |
| 0.45 | 2.09E+12 | 1.19E+12 | 8.86E+11 | 6.86E+11 | 5.35E+11 | 4.18E+11 | 3.27E+11 |
| 0.51 | 2.10E+12 | 1.26E+12 | 9.61E+11 | 7.48E+11 | 5.83E+11 | 4.56E+11 | 3.56E+11 |
| 0.512 | 4.37E+11 | 2.37E+10 | 1.20E+10 | 6.26E+09 | 3.26E+09 | 1.70E+09 | 8.86E+08 |
| 0.6 | 6.77E+12 | 1.13E+12 | 6.35E+11 | 4.42E+11 | 3.24E+11 | 2.43E+11 | 1.86E+11 |
| 0.7 | 3.81E+14 | 2.85E+14 | 2.25E+14 | 1.79E+14 | 1.42E+14 | 1.13E+14 | 8.93E+13 |
| 0.8 | 3.09E+13 | 3.21E+12 | 1.32E+12 | 7.83E+11 | 5.11E+11 | 3.55E+11 | 2.57E+11 |
| 0.9 | 4.27E+12 | 1.61E+12 | 8.95E+11 | 5.52E+11 | 3.66E+11 | 2.57E+11 | 1.88E+11 |
| 1 | 4.37E+12 | 2.13E+12 | 1.10E+12 | 6.02E+11 | 3.58E+11 | 2.29E+11 | 1.56E+11 |
| 1.2 | 3.88E+12 | 1.44E+12 | 8.08E+11 | 5.03E+11 | 3.37E+11 | 2.38E+11 | 1.75E+11 |
| 1.33 | 9.11E+12 | 4.16E+12 | 1.93E+12 | 9.23E+11 | 4.59E+11 | 2.42E+11 | 1.37E+11 |
| 1.44 | 1.68E+12 | 1.56E+11 | 7.86E+10 | 5.86E+10 | 4.50E+10 | 3.48E+10 | 2.70E+10 |
| 1.5 | 2.31E+11 | 1.13E+11 | 6.03E+10 | 3.47E+10 | 2.16E+10 | 1.45E+10 | 1.02E+10 |
| 1.57 | 6.93E+10 | 3.81E+10 | 2.70E+10 | 1.99E+10 | 1.50E+10 | 1.15E+10 | 8.86E+09 |
| 1.66 | 9.13E+11 | 4.22E+11 | 2.01E+11 | 9.93E+10 | 5.20E+10 | 2.92E+10 | 1.77E+10 |
| 1.8 | 4.49E+10 | 2.82E+10 | 2.18E+10 | 1.69E+10 | 1.32E+10 | 1.03E+10 | 8.05E+09 |
| 2 | 2.78E+10 | 1.40E+10 | 1.09E+10 | 8.47E+09 | 6.61E+09 | 5.16E+09 | 4.03E+09 |
| 2.15 | 8.10E+09 | 2.59E+09 | 2.02E+09 | 1.58E+09 | 1.24E+09 | 9.66E+08 | 7.55E+08 |
| 2.35 | 1.50E+10 | 3.43E+07 | 2.21E+07 | 1.61E+07 | 1.18E+07 | 8.73E+06 | 6.54E+06 |
| 2.5 | 7.86E+09 | 1.99E+07 | 8.97E+06 | 7.01E+06 | 5.48E+06 | 4.28E+06 | 3.35E+06 |
| 2.75 | 1.29E+09 | 1.20E+08 | 1.07E+08 | 9.62E+07 | 8.65E+07 | 7.78E+07 | 7.01E+07 |
| 3 | 1.11E+09 | 8.30E+06 | 4.92E+06 | 3.42E+06 | 2.40E+06 | 1.70E+06 | 1.23E+06 |
| 3.5 | 2.84E+08 | 1.00E+07 | 6.73E+06 | 4.68E+06 | 3.29E+06 | 2.33E+06 | 1.68E+06 |
| 4 | 9.65E+06 | 6.51E+06 | 4.50E+06 | 3.13E+06 | 2.20E+06 | 1.56E+06 | 1.12E+06 |
| 4.5 | 6.22E+06 | 4.28E+06 | 2.96E+06 | 2.06E+06 | 1.44E+06 | 1.02E+06 | 7.37E+05 |
| 5 | 4.03E+06 | 2.77E+06 | 1.92E+06 | 1.33E+06 | 9.34E+05 | 6.63E+05 | 4.77E+05 |
| 5.5 | 2.58E+06 | 1.78E+06 | 1.23E+06 | 8.54E+05 | 5.98E+05 | 4.24E+05 | 3.06E+05 |
| 6 | 1.64E+06 | 1.13E+06 | 7.80E+05 | 5.42E+05 | 3.80E+05 | 2.69E+05 | 1.94E+05 |
| 6.5 | 1.03E+06 | 7.11E+05 | 4.91E+05 | 3.42E+05 | 2.39E+05 | 1.70E+05 | 1.22E+05 |
| 7 | 6.47E+05 | 4.45E+05 | 3.08E+05 | 2.14E+05 | 1.50E+05 | 1.06E+05 | 7.64E+04 |
| 7.5 | 4.03E+05 | 2.77E+05 | 1.92E+05 | 1.33E+05 | 9.33E+04 | 6.61E+04 | 4.76E+04 |
| 8 | 2.50E+05 | 1.72E+05 | 1.19E+05 | 8.25E+04 | 5.78E+04 | 4.10E+04 | 2.95E+04 |
| 10 | 3.42E+05 | 2.36E+05 | 1.63E+05 | 1.13E+05 | 7.93E+04 | 5.62E+04 | 4.04E+04 |
| 12 | 2.16E+04 | 1.49E+04 | 1.03E+04 | 7.15E+03 | 5.01E+03 | 3.55E+03 | 2.55E+03 |

**Table A2-3. Gamma radiation intensities for PWR-17x17.**

| Burnup | 40 | | | | | | |
|---|---|---|---|---|---|---|---|
| Power | 4 | | | | | | |
| Case | Real | | | | | | |
| DecayTime | 10 | 20 | 30 | 40 | 50 | 60 | 70 |
| Spectraend | Summa | | | | | | |
| 0.02 | 5.76E+12 | 4.49E+12 | 3.60E+12 | 2.90E+12 | 2.35E+12 | 1.92E+12 | 1.59E+12 |
| 0.03 | 5.14E+12 | 3.80E+12 | 2.98E+12 | 2.35E+12 | 1.86E+12 | 1.48E+12 | 1.18E+12 |
| 0.045 | 1.03E+13 | 7.67E+12 | 5.92E+12 | 4.62E+12 | 3.62E+12 | 2.84E+12 | 2.24E+12 |
| 0.06 | 6.82E+12 | 5.74E+12 | 4.96E+12 | 4.33E+12 | 3.81E+12 | 3.38E+12 | 3.04E+12 |
| 0.07 | 3.40E+12 | 2.59E+12 | 2.02E+12 | 1.57E+12 | 1.23E+12 | 9.63E+11 | 7.54E+11 |
| 0.075 | 1.65E+12 | 1.26E+12 | 9.90E+11 | 7.80E+11 | 6.17E+11 | 4.89E+11 | 3.90E+11 |
| 0.1 | 7.94E+12 | 5.87E+12 | 4.53E+12 | 3.53E+12 | 2.76E+12 | 2.16E+12 | 1.69E+12 |
| 0.15 | 1.43E+13 | 9.75E+12 | 7.11E+12 | 5.35E+12 | 4.10E+12 | 3.17E+12 | 2.47E+12 |
| 0.2 | 1.01E+13 | 7.58E+12 | 5.90E+12 | 4.60E+12 | 3.60E+12 | 2.81E+12 | 2.20E+12 |
| 0.26 | 8.01E+12 | 5.78E+12 | 4.35E+12 | 3.33E+12 | 2.57E+12 | 2.00E+12 | 1.57E+12 |
| 0.3 | 3.99E+12 | 3.06E+12 | 2.39E+12 | 1.87E+12 | 1.47E+12 | 1.15E+12 | 9.08E+11 |
| 0.4 | 1.09E+13 | 8.27E+12 | 6.44E+12 | 5.03E+12 | 3.93E+12 | 3.07E+12 | 2.40E+12 |
| 0.45 | 5.55E+12 | 3.14E+12 | 2.34E+12 | 1.81E+12 | 1.41E+12 | 1.10E+12 | 8.61E+11 |
| 0.51 | 5.57E+12 | 3.32E+12 | 2.53E+12 | 1.97E+12 | 1.54E+12 | 1.20E+12 | 9.38E+11 |
| 0.512 | 1.07E+12 | 5.83E+10 | 2.99E+10 | 1.57E+10 | 8.21E+09 | 4.30E+09 | 2.26E+09 |
| 0.6 | 1.87E+13 | 3.22E+12 | 1.77E+12 | 1.21E+12 | 8.73E+11 | 6.50E+11 | 4.94E+11 |
| 0.7 | 1.03E+15 | 7.73E+14 | 6.12E+14 | 4.85E+14 | 3.85E+14 | 3.06E+14 | 2.43E+14 |
| 0.8 | 8.58E+13 | 9.61E+12 | 3.96E+12 | 2.28E+12 | 1.44E+12 | 9.78E+11 | 6.98E+11 |
| 0.9 | 1.32E+13 | 5.06E+12 | 2.73E+12 | 1.62E+12 | 1.04E+12 | 7.11E+11 | 5.10E+11 |
| 1 | 1.42E+13 | 6.81E+12 | 3.42E+12 | 1.83E+12 | 1.05E+12 | 6.51E+11 | 4.34E+11 |
| 1.2 | 1.17E+13 | 4.39E+12 | 2.39E+12 | 1.44E+12 | 9.39E+11 | 6.50E+11 | 4.70E+11 |
| 1.33 | 2.94E+13 | 1.33E+13 | 6.15E+12 | 2.90E+12 | 1.42E+12 | 7.30E+11 | 4.02E+11 |
| 1.44 | 4.62E+12 | 4.43E+11 | 2.18E+11 | 1.59E+11 | 1.21E+11 | 9.29E+10 | 7.19E+10 |
| 1.5 | 7.69E+11 | 3.69E+11 | 1.91E+11 | 1.06E+11 | 6.35E+10 | 4.10E+10 | 2.82E+10 |
| 1.57 | 1.94E+11 | 1.07E+11 | 7.40E+10 | 5.36E+10 | 4.01E+10 | 3.05E+10 | 2.35E+10 |
| 1.66 | 1.92E+12 | 8.96E+11 | 4.33E+11 | 2.19E+11 | 1.18E+11 | 6.83E+10 | 4.27E+10 |
| 1.8 | 1.17E+11 | 7.44E+10 | 5.75E+10 | 4.47E+10 | 3.48E+10 | 2.72E+10 | 2.12E+10 |
| 2 | 7.01E+10 | 3.63E+10 | 2.84E+10 | 2.22E+10 | 1.73E+10 | 1.36E+10 | 1.06E+10 |
| 2.15 | 2.04E+10 | 6.82E+09 | 5.32E+09 | 4.16E+09 | 3.25E+09 | 2.54E+09 | 1.99E+09 |
| 2.35 | 3.31E+10 | 1.10E+08 | 7.23E+07 | 5.19E+07 | 3.77E+07 | 2.76E+07 | 2.05E+07 |
| 2.5 | 1.93E+10 | 5.09E+07 | 2.36E+07 | 1.84E+07 | 1.44E+07 | 1.13E+07 | 8.82E+06 |
| 2.75 | 3.26E+09 | 4.04E+08 | 3.63E+08 | 3.25E+08 | 2.92E+08 | 2.63E+08 | 2.37E+08 |
| 3 | 2.73E+09 | 2.88E+07 | 1.79E+07 | 1.24E+07 | 8.67E+06 | 6.12E+06 | 4.39E+06 |
| 3.5 | 7.14E+08 | 3.62E+07 | 2.45E+07 | 1.70E+07 | 1.19E+07 | 8.40E+06 | 6.02E+06 |
| 4 | 3.50E+07 | 2.38E+07 | 1.64E+07 | 1.14E+07 | 7.95E+06 | 5.61E+06 | 4.02E+06 |
| 4.5 | 2.27E+07 | 1.56E+07 | 1.08E+07 | 7.46E+06 | 5.21E+06 | 3.68E+06 | 2.63E+06 |
| 5 | 1.47E+07 | 1.01E+07 | 6.97E+06 | 4.83E+06 | 3.38E+06 | 2.38E+06 | 1.70E+06 |
| 5.5 | 9.42E+06 | 6.47E+06 | 4.47E+06 | 3.10E+06 | 2.16E+06 | 1.53E+06 | 1.09E+06 |
| 6 | 5.98E+06 | 4.11E+06 | 2.84E+06 | 1.97E+06 | 1.37E+06 | 9.68E+05 | 6.92E+05 |
| 6.5 | 3.77E+06 | 2.59E+06 | 1.79E+06 | 1.24E+06 | 8.65E+05 | 6.10E+05 | 4.36E+05 |
| 7 | 2.36E+06 | 1.62E+06 | 1.12E+06 | 7.76E+05 | 5.41E+05 | 3.82E+05 | 2.73E+05 |
| 7.5 | 1.47E+06 | 1.01E+06 | 6.97E+05 | 4.83E+05 | 3.37E+05 | 2.38E+05 | 1.70E+05 |
| 8 | 9.11E+05 | 6.26E+05 | 4.32E+05 | 2.99E+05 | 2.09E+05 | 1.47E+05 | 1.05E+05 |
| 10 | 1.25E+06 | 8.58E+05 | 5.92E+05 | 4.10E+05 | 2.87E+05 | 2.02E+05 | 1.44E+05 |
| 12 | 7.89E+04 | 5.42E+04 | 3.74E+04 | 2.59E+04 | 1.81E+04 | 1.28E+04 | 9.11E+03 |

# Appendix 3

## Calculation of deposited energy per voxel

In the data files containing results from Uppsala University's gamma ray simulations, each data record consists of an *x-, y-, z*-coordinate in cm together with a data value of energy in MeV, as described in Chapter 2.2. The coordinate triplet represents the location of an 1 × 1 × 1 cm cubic voxel, whereas the data value shall be interpreted as the expected amount of deposited gamma energy at that voxel per photon of a certain energy emitted from the fuel of the studied configuration at the upright standing canister's horizontal midplane slab of 1 cm thickness. Let's call this data value e, so that

$e = e(x,y,z,\gamma,F)$

where $\gamma$ is the energy of the emitted photon and $F$ is the fuel configuration. For instance, in the data file BWR1_662keV.csv (Table 2-1), the record

30,20,8,2.1424104039769421E−06

tells us that

$e$(30 cm, 20 cm, 8 cm, 662 keV, SVEA96S) = 2.1424104039769421E−06 MeV

Another, perhaps more intuitive, way to interpret the data is to consider the probability

$p = p(x,y,z,\gamma,F) = e/\gamma$

as the probability that a single photon of energy $\gamma$, which is emitted somewhere from the part of the fuel located inside the midplane slab of 1 cm thickness in a canister filled with fuel of configuration $F$, will deposit its energy inside the cubic voxel with its centre located at $x,y,z$.

However, photons are emitted not only from the fuel in the midplane slab, but from all the fuel inside the canister. If we consider the fuel as divided in stacked horisontal slabs with thickness 1 cm, and assume that the fuel part in each of these slabs emits photons with the same spatial distribution as if they were the midplane slab, symmetry yields that the probability that a photon emitted from the midplane slab at $z = 0$ deposit in the voxel at $(x',y',z')$ is equal to the probability that a photon emitted from the slab at $z = -z'$ deposit in the voxel at $(x',y',0)$. Thus, in order to calculate the probability $P$ that a single photon emitted from anywhere in the fuel, i.e from any of the fuel slabs, deposit in the voxel at $(x,y,0)$, the probability contributions from all fuel slabs must be summed from the fuel's bottom to top and be divided by the number of slabs $n$, so that

$$P = P(x,y,0,\gamma,F) = \frac{1}{n}\sum_{z=-n/2}^{n/2} p(x,y,z,\gamma,F)$$

where the fuel height is assumed to be 2 · 184 cm = 368 cm and, consequently, the number of slabs $n$ = 368 running from $z$ = −183 to $z$ = 184 cm.

As an example, $P$(30 cm, 20 cm, 0 cm, 662 keV, SVEA96S) is calculated by summing the $e$-values in Table A3-1 and Table A3-2 and dividing the sum with the number of slabs ($n$ = 368) and the energy of the emitted photon ($\gamma$ = 0.662 MeV), to $P$(30,20,0,662 keV, SVEA96S) = 2.955E−07.

In Table A2-1, the $a$-value, i.e. the number of emitted photons per second, of energy 662 keV, per fuel assembly, for the fuel configuration SVEA96S after 30 years' cooling time, is tabulated to $a$ = 2.28E+14. With 12 fuel assemblies of SVEA96S in the canister, the heat power $q$ in the voxel at $(x,y,z)$ = (30,20,0) is calculated to $q$(30,20,0,662keV,SVEA96S) = 2.955E−07 · 662keV · 12 · 2.28E+14 = 5.35E+11 keV = 8.57E−5 W, or 85.7 W/m$^3$, assuming that all deposited gamma energy transforms to heat.

**Table A3-1. Data records from BWR1_662keV.csv for (x,y)=(30,20) z=[−184,(−1)] cm.**

| z (cm) | e (MeV) | z (cm) | e (MeV) | z (cm) | e (MeV) | z (cm) | e (MeV) |
|---|---|---|---|---|---|---|---|
| −184 | 9.265E−14 | −138 | 5.681E−13 | −92 | 7.579E−12 | −46 | 5.068E−10 |
| −183 | 2.573E−13 | −137 | 6.479E−13 | −91 | 7.802E−12 | −45 | 5.890E−10 |
| −182 | 1.976E−13 | −136 | 1.008E−12 | −90 | 8.386E−12 | −44 | 6.693E−10 |
| −181 | 1.008E−13 | −135 | 8.604E−13 | −89 | 9.300E−12 | −43 | 7.761E−10 |
| −180 | 1.579E−13 | −134 | 1.047E−12 | −88 | 9.843E−12 | −42 | 9.033E−10 |
| −179 | 2.079E−13 | −133 | 8.750E−13 | −87 | 1.072E−11 | −41 | 1.045E−09 |
| −178 | 1.620E−13 | −132 | 9.035E−13 | −86 | 1.096E−11 | −40 | 1.227E−09 |
| −177 | 2.512E−13 | −131 | 1.019E−12 | −85 | 1.199E−11 | −39 | 1.433E−09 |
| −176 | 1.849E−13 | −130 | 1.135E−12 | −84 | 1.289E−11 | −38 | 1.679E−09 |
| −175 | 2.068E−13 | −129 | 9.425E−13 | −83 | 1.329E−11 | −37 | 1.962E−09 |
| −174 | 2.581E−13 | −128 | 1.095E−12 | −82 | 1.481E−11 | −36 | 2.305E−09 |
| −173 | 2.178E−13 | −127 | 9.739E−13 | −81 | 1.599E−11 | −35 | 2.725E−09 |
| −172 | 2.084E−13 | −126 | 1.044E−12 | −80 | 1.778E−11 | −34 | 3.230E−09 |
| −171 | 1.757E−13 | −125 | 1.211E−12 | −79 | 1.828E−11 | −33 | 3.826E−09 |
| −170 | 1.685E−13 | −124 | 1.227E−12 | −78 | 2.048E−11 | −32 | 4.570E−09 |
| −169 | 2.593E−13 | −123 | 1.246E−12 | −77 | 2.141E−11 | −31 | 5.473E−09 |
| −168 | 1.668E−13 | −122 | 1.336E−12 | −76 | 2.429E−11 | −30 | 6.576E−09 |
| −167 | 1.966E−13 | −121 | 1.391E−12 | −75 | 2.580E−11 | −29 | 7.979E−09 |
| −166 | 3.416E−13 | −120 | 1.390E−12 | −74 | 2.808E−11 | −28 | 9.725E−09 |
| −165 | 1.777E−13 | −119 | 2.154E−12 | −73 | 3.013E−11 | −27 | 1.192E−08 |
| −164 | 2.095E−13 | −118 | 2.054E−12 | −72 | 3.245E−11 | −26 | 1.476E−08 |
| −163 | 2.384E−13 | −117 | 1.995E−12 | −71 | 3.446E−11 | −25 | 1.839E−08 |
| −162 | 2.804E−13 | −116 | 2.062E−12 | −70 | 3.906E−11 | −24 | 2.310E−08 |
| −161 | 3.751E−13 | −115 | 1.959E−12 | −69 | 4.152E−11 | −23 | 2.924E−08 |
| −160 | 4.011E−13 | −114 | 2.192E−12 | −68 | 4.483E−11 | −22 | 3.719E−08 |
| −159 | 3.215E−13 | −113 | 2.114E−12 | −67 | 4.934E−11 | −21 | 4.760E−08 |
| −158 | 3.660E−13 | −112 | 2.316E−12 | −66 | 5.510E−11 | −20 | 6.155E−08 |
| −157 | 2.838E−13 | −111 | 2.567E−12 | −65 | 6.001E−11 | −19 | 8.045E−08 |
| −156 | 2.995E−13 | −110 | 2.814E−12 | −64 | 6.628E−11 | −18 | 1.064E−07 |
| −155 | 4.445E−13 | −109 | 2.571E−12 | −63 | 7.244E−11 | −17 | 1.423E−07 |
| −154 | 3.344E−13 | −108 | 2.965E−12 | −62 | 7.913E−11 | −16 | 1.924E−07 |
| −153 | 4.005E−13 | −107 | 3.713E−12 | −61 | 8.814E−11 | −15 | 2.625E−07 |
| −152 | 4.030E−13 | −106 | 3.249E−12 | −60 | 9.616E−11 | −14 | 3.621E−07 |
| −151 | 3.947E−13 | −105 | 3.289E−12 | −59 | 1.077E−10 | −13 | 5.046E−07 |
| −150 | 3.770E−13 | −104 | 3.656E−12 | −58 | 1.222E−10 | −12 | 7.096E−07 |
| −149 | 3.312E−13 | −103 | 3.926E−12 | −57 | 1.330E−10 | −11 | 1.013E−06 |
| −148 | 5.102E−13 | −102 | 4.055E−12 | −56 | 1.479E−10 | −10 | 1.467E−06 |
| −147 | 5.797E−13 | −101 | 4.391E−12 | −55 | 1.644E−10 | −9 | 2.143E−06 |
| −146 | 4.857E−13 | −100 | 4.800E−12 | −54 | 1.872E−10 | −8 | 3.162E−06 |
| −145 | 5.368E−13 | −99 | 4.589E−12 | −53 | 2.072E−10 | −7 | 4.699E−06 |
| −144 | 5.159E−13 | −98 | 5.738E−12 | −52 | 2.344E−10 | −6 | 7.512E−06 |
| −143 | 6.807E−13 | −97 | 5.416E−12 | −51 | 2.662E−10 | −5 | 1.120E−05 |
| −142 | 6.208E−13 | −96 | 5.831E−12 | −50 | 3.000E−10 | −4 | 1.313E−06 |
| −141 | 7.612E−13 | −95 | 6.173E−12 | −49 | 3.404E−10 | −3 | 4.752E−07 |
| −140 | 5.539E−13 | −94 | 6.993E−12 | −48 | 3.886E−10 | −2 | 2.127E−07 |
| −139 | 6.382E−13 | −93 | 7.416E−12 | −47 | 4.410E−10 | −1 | 1.280E−07 |

**Table A3-2. Data records from BWR1_662keV.csv for (x,y)=(30,20) z=[0.183] cm.**

| z (cm) | e (MeV) | z (cm) | e (MeV) | z (cm) | e (MeV) | z (cm) | e (MeV) |
|---|---|---|---|---|---|---|---|
| 0 | 1.281E−07 | 46 | 4.446E−10 | 92 | 7.557E−12 | 138 | 5.263E−13 |
| 1 | 2.127E−07 | 47 | 3.854E−10 | 93 | 6.570E−12 | 139 | 5.710E−13 |
| 2 | 4.752E−07 | 48 | 3.421E−10 | 94 | 6.310E−12 | 140 | 6.452E−13 |
| 3 | 1.313E−06 | 49 | 2.937E−10 | 95 | 5.563E−12 | 141 | 4.835E−13 |
| 4 | 1.120E−05 | 50 | 2.643E−10 | 96 | 5.284E−12 | 142 | 6.041E−13 |
| 5 | 7.512E−06 | 51 | 2.338E−10 | 97 | 5.295E−12 | 143 | 5.029E−13 |
| 6 | 4.699E−06 | 52 | 2.111E−10 | 98 | 4.312E−12 | 144 | 7.012E−13 |
| 7 | 3.161E−06 | 53 | 1.858E−10 | 99 | 5.162E−12 | 145 | 4.056E−13 |
| 8 | 2.142E−06 | 54 | 1.670E−10 | 100 | 4.559E−12 | 146 | 5.261E−13 |
| 9 | 1.467E−06 | 55 | 1.478E−10 | 101 | 4.263E−12 | 147 | 5.676E−13 |
| 10 | 1.012E−06 | 56 | 1.319E−10 | 102 | 3.948E−12 | 148 | 4.829E−13 |
| 11 | 7.098E−07 | 57 | 1.197E−10 | 103 | 3.773E−12 | 149 | 4.768E−13 |
| 12 | 5.046E−07 | 58 | 1.093E−10 | 104 | 3.485E−12 | 150 | 4.815E−13 |
| 13 | 3.620E−07 | 59 | 9.845E−11 | 105 | 3.208E−12 | 151 | 3.822E−13 |
| 14 | 2.624E−07 | 60 | 8.809E−11 | 106 | 2.952E−12 | 152 | 3.651E−13 |
| 15 | 1.923E−07 | 61 | 7.956E−11 | 107 | 3.355E−12 | 153 | 4.091E−13 |
| 16 | 1.424E−07 | 62 | 7.218E−11 | 108 | 3.121E−12 | 154 | 2.784E−13 |
| 17 | 1.065E−07 | 63 | 6.490E−11 | 109 | 2.925E−12 | 155 | 3.342E−13 |
| 18 | 8.044E−08 | 64 | 6.051E−11 | 110 | 2.837E−12 | 156 | 3.483E−13 |
| 19 | 6.153E−08 | 65 | 5.438E−11 | 111 | 2.311E−12 | 157 | 2.529E−13 |
| 20 | 4.762E−08 | 66 | 4.837E−11 | 112 | 2.064E−12 | 158 | 2.243E−13 |
| 21 | 3.718E−08 | 67 | 4.437E−11 | 113 | 2.122E−12 | 159 | 3.740E−13 |
| 22 | 2.920E−08 | 68 | 4.188E−11 | 114 | 2.135E−12 | 160 | 3.210E−13 |
| 23 | 2.313E−08 | 69 | 3.841E−11 | 115 | 1.912E−12 | 161 | 2.419E−13 |
| 24 | 1.840E−08 | 70 | 3.489E−11 | 116 | 1.842E−12 | 162 | 3.458E−13 |
| 25 | 1.474E−08 | 71 | 3.305E−11 | 117 | 1.717E−12 | 163 | 4.193E−13 |
| 26 | 1.192E−08 | 72 | 2.977E−11 | 118 | 1.684E−12 | 164 | 2.786E−13 |
| 27 | 9.690E−09 | 73 | 2.628E−11 | 119 | 1.583E−12 | 165 | 2.130E−13 |
| 28 | 7.981E−09 | 74 | 2.627E−11 | 120 | 1.424E−12 | 166 | 2.338E−13 |
| 29 | 6.594E−09 | 75 | 2.297E−11 | 121 | 1.442E−12 | 167 | 2.451E−13 |
| 30 | 5.457E−09 | 76 | 2.183E−11 | 122 | 1.340E−12 | 168 | 1.941E−13 |
| 31 | 4.574E−09 | 77 | 2.015E−11 | 123 | 1.360E−12 | 169 | 2.164E−13 |
| 32 | 3.829E−09 | 78 | 1.899E−11 | 124 | 1.392E−12 | 170 | 1.501E−13 |
| 33 | 3.232E−09 | 79 | 1.619E−11 | 125 | 1.173E−12 | 171 | 1.319E−13 |
| 34 | 2.733E−09 | 80 | 1.632E−11 | 126 | 1.190E−12 | 172 | 2.703E−13 |
| 35 | 2.325E−09 | 81 | 1.501E−11 | 127 | 1.238E−12 | 173 | 1.316E−13 |
| 36 | 1.963E−09 | 82 | 1.365E−11 | 128 | 1.135E−12 | 174 | 1.978E−13 |
| 37 | 1.675E−09 | 83 | 1.336E−11 | 129 | 9.098E−13 | 175 | 1.870E−13 |
| 38 | 1.423E−09 | 84 | 1.162E−11 | 130 | 8.528E−13 | 176 | 1.153E−13 |
| 39 | 1.215E−09 | 85 | 1.116E−11 | 131 | 1.070E−12 | 177 | 2.252E−13 |
| 40 | 1.049E−09 | 86 | 1.067E−11 | 132 | 8.635E−13 | 178 | 2.323E−13 |
| 41 | 9.090E−10 | 87 | 9.712E−12 | 133 | 8.933E−13 | 179 | 1.530E−13 |
| 42 | 7.763E−10 | 88 | 9.008E−12 | 134 | 7.260E−13 | 180 | 1.905E−13 |
| 43 | 6.712E−10 | 89 | 8.724E−12 | 135 | 6.240E−13 | 181 | 1.802E−13 |
| 44 | 5.858E−10 | 90 | 8.391E−12 | 136 | 6.806E−13 | 182 | 1.296E−13 |
| 45 | 5.037E−10 | 91 | 7.107E−12 | 137 | 6.913E−13 | 183 | 1.342E−13 |

Arkitektkopia AB, Bromma, 2020

SKB is responsible for managing spent nuclear fuel and radioactive waste produced by the Swedish nuclear power plants such that man and the environment are protected in the near and distant future.

**skb.se**